

Nanoscale Surface Compositions and Structures Influence Boron Adsorption Properties of Anion Exchange Resins

G. N. Manjunatha Reddy,[†] Jeffrey A. Gerbec,[‡] Fumihiko Shimizu,[§] and Bradley F. Chmelka^{*,†}

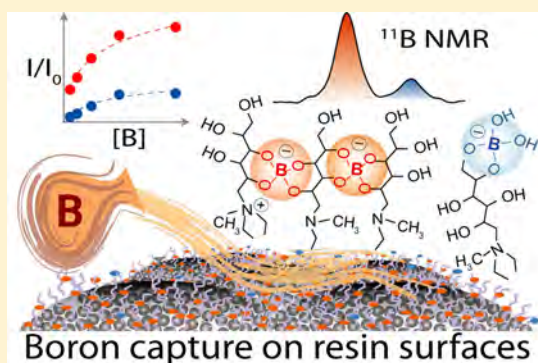
[†]Department of Chemical Engineering, University of California, Santa Barbara, Santa Barbara, California 93106, United States

[‡]Mitsubishi Chemical–Center for Advanced Materials, University of California, Santa Barbara, Santa Barbara, California 93106, United States

[§]Science and Innovation Center, Mitsubishi Chemical Corporation, Yokohama-shi, Kanagawa 227-8502, Japan

Supporting Information

ABSTRACT: Boron adsorption properties of poly(styrene-*co*-divinylbenzene) (PSDVB)-based anion-exchange resins with surface-grafted *N*-methyl-*D*-glucamine (NMDG) depend strongly on their local surface compositions, structures, and interfacial interactions. Distinct boron adsorption sites have been identified and quantified, and interactions between borate anions and hydroxyl groups of NMDG surface moieties have been established. A combination of X-ray photoelectron spectroscopy (XPS), solid-state nuclear magnetic resonance (NMR), and Fourier-transform infrared (FT-IR) spectroscopy were used to characterize the atomic-level compositions and structures that directly influence the adsorption of borate anions on the NMDG-functionalized resin surface. Surface-enhanced dynamic-nuclear-polarization (DNP)-NMR enabled dilute (3 atom % N) tertiary alkyl amines and quaternary ammonium ions of the NMDG groups to be detected and distinguished with unprecedented sensitivity and resolution at natural abundance ¹⁵N (0.4%). Two-dimensional (2D) solid-state ¹¹B{¹H}, ¹³C{¹H}, and ¹¹B{¹B} NMR analyses provide direct atomic-scale evidence for interactions of borate anions with the NMDG moieties on the resin surfaces, which form stable mono- and bischelate complexes. FT-IR spectra reveal displacements in the stretching vibrational frequencies associated with the O–H and N–H bonds of NMDG groups that corroborate the formation of chelate complexes on the resin surfaces. The atomic-level compositions and structures are related to boron adsorption properties of resin materials synthesized under different conditions, which have important remediation applications.



INTRODUCTION

Highly cross-linked polymers with surface-grafted acidic or basic functional groups are used to adsorb and exchange counterions from aqueous and organic solutions. The ion-exchange properties of such polymer resins can be adjusted by incorporating suitable surface functional groups for different technological applications including desalination,^{1,2} chromatography-based separation and purification,³ and catalysis.^{4–6} For example, naturally occurring chitosan polymers or synthetic styrene-divinylbenzene copolymers grafted with surface COO[−] or SO₃[−] functional groups have been shown to exchange cations¹ or anions^{7–9} when surface-grafted with sorbitol,¹⁰ mannitol,¹¹ and *N*-methyl-*D*-glucamine (NMDG) groups.^{12,13} Ion-exchange resins have also been used to catalyze reactions, such as alkylation, isomerization, oligomerization, acylation, esterification, and nitration^{14–16} and have long been recognized for their environmental remediation applications.^{8,12,13,17,18} Of particular interest, ion-exchange resins have been used to reduce boron concentration levels in soil, surface, and wastewaters, including as part of decontamination efforts in Fukushima, Japan. Boron-containing materials are also used extensively in power generation

applications¹⁹ and in the production and processing of diverse engineering materials, such as glasses, ceramics, fertilizers, detergents, catalysts, and semiconductors.^{20–23} Despite their high technological importance, much remains unknown about the relationships between the compositions, structures, and properties of boron-containing materials, especially those involving dilute surface species.

In particular, many commercial boron-adsorption ion-exchange resins are based on polymers grafted with NMDG functional groups.^{12,13,24,25} For such materials, the hydroxyl groups of the NMDG moieties exhibit high binding affinity toward borate anions.^{20,26} This imparts the NMDG-functionalized polymers with high boron adsorption capacities and correspondingly favorable separation efficiencies, compared to other approaches such as reverse osmosis,^{27,28} electrodialysis,²⁹ polymer-enhanced ultrafiltration,³⁰ and sorption,^{31,32} which

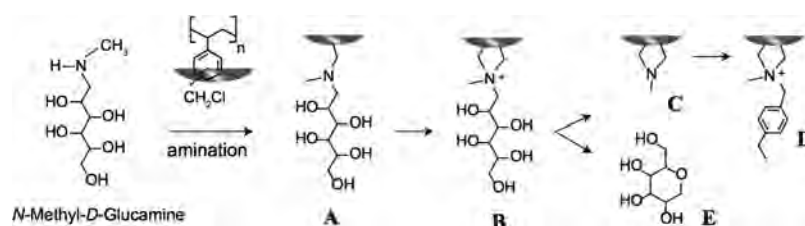
Special Issue: Intermolecular Forces and Interfacial Science

Received: July 2, 2019

Revised: August 14, 2019

Published: September 3, 2019

Scheme 1. Schematic Diagrams of Different Amination Products That May Be Present on the Surfaces of PSDVB and NMDG Surface-Grafted Resins^a



^a(A,C) Tertiary and (B,D) quaternary ammonium moieties with (A,B) and without (C,D) polyhydroxyl groups and (E) a sugarlike species.

tend to rely on weak noncovalent interactions. The reversible interactions of borate anions with hydroxyl groups have been exploited in the development of boron sorbents based on nitrogen-doped graphene oxide surface-grafted with hydroxyl groups,³³ diol-functionalized silica particles,³⁴ and Nylon-6 fibrils grafted with NMDG moieties.³⁵ The resulting boron-adsorption properties of ion-exchange resins depend strongly on their surface compositions and structures and also on reaction conditions, such as, pH, temperature, concentration, diffusion, and the transport properties of exchangeable ions. While reaction conditions can be adjusted to improve the boron-adsorption properties of the resins, molecular-level understanding of how their surface compositions and structures influence or account for such properties has been limited. This has been due, in part to (i) poor solubility of the resins in aqueous or organic solvents, which makes solution-state characterization methods impractical, and (ii) the heterogeneity of resin surfaces, which limits the utility of X-ray scattering, electron microscopy, and standard surface characterization methods. Nevertheless, boron-adsorbing resins have been characterized by Fourier-transform infrared (FT-IR) spectroscopy, scanning electron microscopy (SEM), mass spectrometry (MS), and NMR spectroscopy.²⁴ Such methods provide structural information on complementary length and time scales, though until now they have provided limited insights on site-specific molecular-level interactions and adsorption behaviors of borate anions adsorbed on the heterogeneous resin surfaces. It has been hypothesized that boron adsorption occurs by forming chelate complexes between borate anions and hydroxyl groups of NMDG moieties on the polymer surface,^{24,25} although little direct evidence has been available to date to establish the interactions between borate anions and surface functional groups.

The nanoscale sensitivity and resolution of solid-state NMR spectroscopy enables site-specific molecular interactions and structures to be measured and distinguished in heterogeneous materials lacking long-range structural order.^{36–39} In particular, interatomic proximities between dipole–dipole-coupled nuclei can be established by analyses of powerful 2D correlation NMR spectra. Recently, one-dimensional (1D) solid-state ¹¹B MAS NMR has been used to probe local boron environments in chelate complexes of ion-exchange resins and supramolecular hydrogels.^{40,41} Similar analyses of solid-state 1D ¹H and ¹³C MAS NMR spectra have yielded insights on surface compositions and structures of ion-exchange resins, though the signals are often poorly resolved, due to distributions of species associated with the polymer substrate (e.g., polystyrene) and surface-grafted NMDG functional groups. In principle, the use of solid-state ¹⁵N MAS NMR can also provide information on ¹⁵N-containing surface moieties with improved resolution,

though it is rarely used because of the low natural isotopic abundance of ¹⁵N (0.4%) and the often-low elemental contents of ¹⁵N (<5 atom %) at NMDG-functionalized resin surfaces. Crucially, DNP-enhanced solid-state NMR provides large sensitivity enhancements that enable surface compositions, structures, and properties of ¹⁵N-containing surface moieties to be detected and analyzed with unprecedented sensitivity and resolution, including for natural abundance ¹⁵N. DNP-NMR techniques have been used to characterize the surface structures and properties of zeolites and supported catalysts, hydration properties of cements, porous solids, and polymers,^{42–51} which were previously infeasible by using conventional NMR or other methods.

Here, complementary X-ray photoelectron spectroscopy (XPS) and solid-state surface-enhanced DNP-NMR analyses were conducted to elucidate the local surface compositions and structures of NMDG-functionalized resins, as functions of their syntheses and boron-adsorption conditions. The molecular-level proximities and structures of chelate complexes on the resin surfaces can be established by using powerful 2D ¹H{¹H}, ¹¹B{¹H}, ¹¹B{¹¹B}, and ¹³C{¹H} correlation NMR techniques. These enable different types of boron adsorption sites on the resin surface to be identified, which can subsequently be quantified by using direct-excitation 1D ¹¹B MAS NMR. The results yield new quantitative insights on surface compositions and site-specific boron interactions that account for the boron-adsorption properties of the anion-exchange resins.

EXPERIMENTAL SECTION

Materials and Methods. Poly(styrene-*co*-divinylbenzene) (PSDVB) resin and *N*-methyl-*D*-glucamine (NMDG) were purchased from Sigma-Aldrich and used as-received. DIAION CRB03 resins were used as a representative case study, because different batches can exhibit significantly different boron-adsorption properties. Different DIAION CRB03 ion-exchange resins, each before and after exposure to boron, were obtained from Mitsubishi Chemical Co. and used as-received. DIAION CRB03 is a special grade of boron ion-exchange resin that adsorbs boron at low concentrations and has an adsorption capacity of 15–29 mg of boron per 1 g of NMDG-functionalized resin. DIAION CRB03 boron-adsorbing resins are generally synthesized by chloromethylation of polystyrene, followed by amination with NMDG moieties as shown in Scheme 1.

Characterization. SEM micrographs were obtained at room temperature using a FEI XL40 Sirion FEG digital scanning electron microscope at 40 000× magnification and 7 kV electron beam voltage (Figure 1a). Powder X-ray diffraction (XRD) experiments were performed at room temperature on a PANalytical Empyrean Multi-Function powder diffractometer using Cu K α radiation with a wavelength of 1.54 Å. Powder patterns were acquired by varying 2θ angles between 5° and 60° that were scanned at a rate of 12°/min. The powder X-ray diffraction pattern (Figure 1b) of the boron-

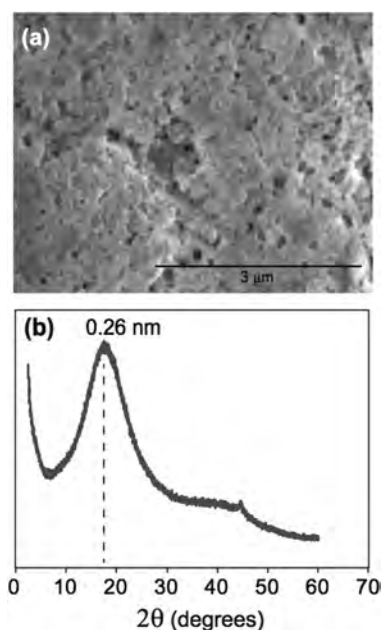


Figure 1. (a) SEM image of a boron-adsorbed NMDG-functionalized resin with the specifications given in Table 1. The micrograph was acquired at room temperature using a 7 kV electron beam and at 40 000 \times magnification. (b) Powder XRD pattern of the same resin measured at room temperature exhibiting a broad reflection centered at 17 $^\circ$, corresponding to a d -spacing of 0.26 nm associated with the strong π - π interactions between PSDVB backbone moieties.

adsorbed resin exhibits a broad reflection centered at 17 $^\circ$ (d -spacing of 0.26 nm, as calculated from Bragg's law), which is associated with strong π - π stacking interactions of the PSDVB moieties. XPS measurements were conducted at room temperature on a Kratos Axis Ultra X-ray photoelectron spectrometer. Survey XPS sweeps were acquired over the range of 800–100 eV with a pass energy of 160 eV in increments of 0.5 eV; high-resolution XPS scans were conducted for O 1s (541–525 eV), C 1s (296–276 eV), and N 1s (410–390 eV) with a pass energy of 40 eV and a step size of 0.05 eV. Elemental compositions of surface C, O, N, and B atoms were estimated by the deconvolution of XPS signal intensities with Gaussian distributions using Casa XPS 2.3.15 software (Casa Software Ltd., Teignmouth, Devon, U.K.), corresponding to O (532.8 \pm 0.3 eV), N (402–399 eV), C (284–292 eV), and B (191.7 \pm 0.4 eV) moieties. Concentrations of borate anions and metal ions were determined by using inductively coupled plasma (ICP) optimal emission spectroscopy (Table S1). Solid-state FT-IR experiments were carried out at room temperature using a Thermo Scientific Nicolet iS10 FT-IR spectrometer equipped with a smart diamond attenuated total reflectance (SD-ATR) accessory to acquire mid-infrared range frequencies between 4000 and 500 cm^{-1} . Physicochemical properties such as porosity, mean particle size, surface area, and salt-splitting capacity of the DIAION CRB03 series resins are given in Table 1. The salt-splitting capacity was determined by titrating resin surfaces containing quaternary ammonium ions with counteranions.⁵²

Surface-Enhanced DNP-NMR Spectroscopy. The local ^{15}N environments of functional moieties on the resin surfaces were characterized by using surface-enhanced $^{15}\text{N}\{^1\text{H}\}$ cross-polarization (CP)-magic-angle spinning (MAS) DNP-NMR spectroscopy. DNP-NMR techniques exploit electron spin polarization transferred to nuclear spins via hyperfine interactions at low temperature (here, 92 K) by continuously irradiating electron spins with microwaves at the electron Larmor frequency (263 GHz at 9.4 T). In principle, such polarization transfer can yield NMR signal enhancements according to the ratio of γ_e/γ_n , where γ_e and γ_n are the respective gyromagnetic ratios of the electron and nuclear spins. This leads to theoretical sensitivity gains of up to ~ 660 , ~ 2600 , and ~ 6600 for ^1H , ^{13}C , and

Table 1. Physicochemical Properties of Boron Adsorbing Anion Exchange Resins^a

property	before boron exposure	after boron exposure
boron content (ppm)	0.1	2500
total exchange capacity (A + B + C + D) (mmol/g)	2.73	2.73
salt splitting capacity (B + D, mmol/g)	0.52	0.52
specific surface area (m^2/g)	35	35
pore radius (nm)	30	30
mean particle size (mm)	0.56	0.56

^aSchematic structures of A, B, C and D are shown in Scheme 1.

^{15}N nuclei, respectively, which opens new opportunities for analyzing surface compositions for a range of functional materials. The observed sensitivity gains, however, depend on material compositions, the type of polarizing radical, solvent, temperature, microwave power and magnetic field strengths. Samples for DNP-enhanced ^{15}N NMR experiments were prepared by the incipient wetness method,^{45,53–56} a combination of 20 mg of resin and 20 μL of 16 mM TEKPol in 1,1,2,2-tetrachloroethane (TCE)^{55,57} was thoroughly mixed using a glass rod at room temperature to ensure macroscopically uniform distribution of the polarizing biradicals on the resin surfaces, resulting in a pastelike sample.^{45,53–55} The sample was then immediately transferred into a 3.2 mm (outer diameter) sapphire MAS rotor, sealed with a polytetrafluoroethylene insert, fitted with a Vespel rotor cap, and inserted into the precooled DNP-NMR probehead. All solid-state DNP-NMR measurements were conducted on freeze-dried resin samples (92 K) on a 9.4 T Bruker AVANCE-III NMR spectrometer (^1H , 399.95 MHz and ^{15}N , 40.6 MHz) equipped with a Bruker 3.2 mm H-X-Y triple resonance variable-temperature MAS probehead, a cooling cabinet and a 263 GHz gyrotron microwave source and waveguide system operating at 120 mA of continuous microwave irradiation.⁵⁸ Surface-enhanced 1D $^{13}\text{C}\{^1\text{H}\}$ and $^{15}\text{N}\{^1\text{H}\}$ DNP-NMR spectra were acquired using 2 ms of CP contact time with SPINAL-64 heteronuclear $^{13}\text{C}\{^1\text{H}\}$ decoupling under 8 kHz MAS. The ^1H and ^{13}C 90 $^\circ$ radiofrequency pulse durations were 2.5 and 4 μs , respectively. The DNP-enhanced $^{13}\text{C}\{^1\text{H}\}$ CP-MAS signals (Figure 2a) from the TCE solvent (73 ppm) and resin ^{13}C nuclei (39 ppm) increased initially to a TEKPol concentration of 15–20 mM, yielding maxima of $\epsilon_{\text{solvent}} = 162$ and $\epsilon_{\text{resin}} = 45$ (relative to the intensities of the same signals in the absence of microwave irradiation under otherwise identical conditions, Figure 2b).⁴² For higher TEKPol concentrations, the signal enhancements decreased, due to paramagnetic broadening or shorter spin–lattice relaxation times. Notably, DNP-enhanced conditions enabled the detection of $^{15}\text{N}\{^1\text{H}\}$ CP-MAS spectra (Figure 2c) on natural abundance ^{15}N (0.4%) in 18 h ($\epsilon_{\text{resin}} = 12$). This facilitated the direct measurement, resolution, and identification of ^{15}N signals from tertiary amines and quaternary ammonium ions, even at a dilute near-surface elemental concentration of 3 atom % N.

Solid-State MAS NMR. To identify distinct boron adsorption sites and to establish boron-resin surface interactions, conventional solid-state ^1H , ^{11}B and ^{13}C MAS NMR spectra of NMDG, polystyrene and the resins were acquired and analyzed. Samples were separately packed into 4 mm (outer diameter) zirconia rotors and fitted with Kel-F caps. All 1D $^{13}\text{C}\{^1\text{H}\}$ and $^{11}\text{B}\{^1\text{H}\}$ CP-MAS spectra and 2D $^{13}\text{C}\{^1\text{H}\}$ and 2D $^{11}\text{B}\{^1\text{H}\}$ heteronuclear correlation (HETCOR) spectra were acquired at room temperature on a 11.7 T Bruker AVANCE-II NMR spectrometer (^1H 500 MHz ^{11}B 160 MHz, and ^{13}C 125 MHz) using a 4 mm H-X-Y MAS probe head. The nutation frequencies for ^1H , ^{13}C , and ^{11}B nuclei were 100, 83, and 83 kHz, corresponding to 90 $^\circ$ pulse lengths of 2.5, 3, and 3 μs , respectively. The spin–lattice relaxation times (T_1) of ^1H and ^{11}B nuclei were determined to be 3 and 30 s, respectively, based on inversion–recovery measurements and analyses. 1D $^{13}\text{C}\{^1\text{H}\}$ and $^{11}\text{B}\{^1\text{H}\}$ CP-MAS experiments were acquired at 8 kHz MAS, with a CP contact time of 2 ms by coadding 1024 transients with a ^1H recycle delay of 3

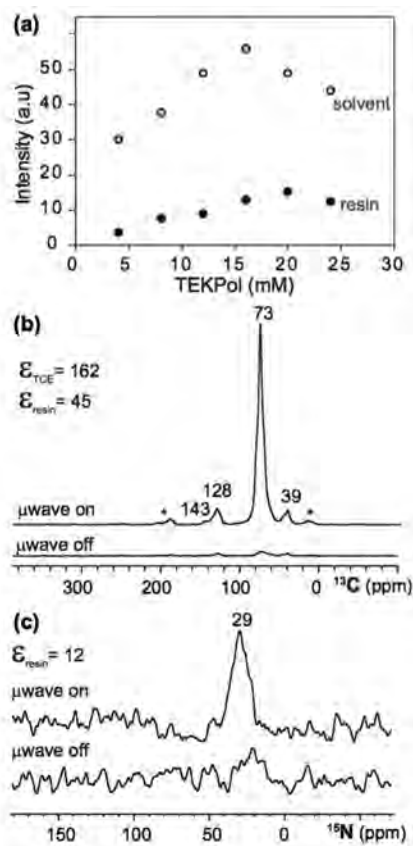


Figure 2. (a) DNP-enhanced 1D $^{13}\text{C}\{^1\text{H}\}$ CP-MAS signal intensities of the TCE solvent and poly(styrene-co-divinylbenzene) (PSDVB) resin plotted, as functions of the concentration of the TEKPol biradical in 1,1,2,2-tetrachloroethane. Comparison of (b) 1D $^{13}\text{C}\{^1\text{H}\}$ and (c) 1D $^{15}\text{N}\{^1\text{H}\}$ CP-MAS NMR spectra of boron-exposed anion exchange resins acquired at 92 K using 16 mM TEKPol in 1,1,2,2-tetrachloroethane in the presence and absence of microwave (MW) irradiation. DNP enhancements of 45 and 12 are measured for the $^{13}\text{C}\{^1\text{H}\}$ and $^{15}\text{N}\{^1\text{H}\}$ CP-MAS signal intensities, respectively, of the resin materials. Asterisks denote spinning sidebands.

s, corresponding to a total experimental time of 1 h each. To understand the borate adsorption behaviors, 50 mg boron-free resin beads were soaked in different vials containing 1 mL of aqueous solutions of 8, 4, 2, 1, and 0.5 g/L boric acid at ambient conditions for 2 h. Boron-exposed resin beads were subsequently filtered and dried at room temperature for 2 days, and the solid-state $^{11}\text{B}\{^1\text{H}\}$ CP-MAS NMR experiments were carried out. 2D $^{13}\text{C}\{^1\text{H}\}$ and $^{11}\text{B}\{^1\text{H}\}$ HETCOR spectra were recorded at 12.5 kHz MAS with a CP contact time of 2 ms and 40 t_1 increments, each with 64 coadded transients, using incremental steps of 80 μs , and a recycle delay of 4 s, corresponding to a total experimental time of 4 h each.

All fast (60 kHz) ^1H and ^{11}B MAS NMR experiments were conducted at 11.7 T and at room temperature using a 1.3 mm H-X double resonance MAS probehead. Samples of NMDG, PSDVB resin and boron-adsorbed NMDG-functionalized resin were separately packed into 1.3 mm rotors fitted with Vespel caps. Single-pulse (direct-excitation) ^1H MAS NMR experiments were carried out by coadding 16 transients with a recycle delay of 3 s, resulting in a total experimental time of 2 min each. 2D ^1H double-quantum (DQ) single-quantum (SQ) spectra were acquired using the Back-to-Back (BaBa) sequence with one rotor period.⁵⁹ The DQ coherences were excited and reconverted using a 16-step phase cycle that incorporated $\Delta p = \pm 2$ on the DQ excitation pulses (4 steps) and $\Delta p = \pm 1$ (4 steps) on the z-filter 90° pulse, where p is the coherence order. 2D data were acquired using 128 t_1 increments, each with 16 coadded

transients, a 3 s recycle delay, and using the States method to achieve sign discrimination in the indirect dimension with a rotor-synchronized t_1 increment of 13.3 μs , resulting in a total experimental time of 2 h. For boron-exposed resins, quantitative single-pulse ^{11}B MAS NMR spectra were acquired by using 400 coadded transients and a recycle delay of 30 s, corresponding to a total experimental time of 3.3 h. The 2D $^{11}\text{B}\{^1\text{H}\}$ dipolar-correlation NMR spectrum of boron-adsorbed NMDG-functionalized PSDVB resin was acquired at 20 T (850 MHz for ^1H), 298 K, and 25 kHz MAS.

The ^1H and ^{13}C chemical shifts were calibrated with respect to neat TMS using adamantane as an external reference with a ^1H chemical shift of 1.85 ppm and ^{13}C shifts of 29.5 and 38.6 ppm. ^{11}B chemical shifts were calibrated with respect to the ^{11}B shift for $\text{NaB}(\text{OH})_4$ at -49.5 ppm using neat $\text{BF}_3(\text{OC}_2\text{H}_5)_3$ as an external reference with a ^{11}B shift of 0 ppm. ^{15}N chemical shifts were referenced to neat CH_3NO_2 by using powdered NH_4Cl at -341.2 as an external reference (Table 2 of ref 60). To convert to the chemical shift scale frequently used in protein NMR analyses, where the alternative IUPAC (Appendix 1 of ref 61) reference is liquid NH_3 at -50°C , it is necessary to add 379.5 ppm to the given values.⁶²

RESULTS AND DISCUSSION

Local Surface Compositions of Anion Exchange Resins. Determining the local surface compositions of boron-exchange resins, such as DIAION CRB03, and in particular the interactions of functional groups with adsorbed boron, is of high interest for understanding the origins of their interesting separation properties. Because the surface heterogeneities associated with NMDG-functionalized PSDVB resins exhibit little to no long-range structural order, diffraction-based techniques are generally not able to distinguish and identify surface functional groups (Scheme 1). By comparison, analyses of survey-scan (Figure 3a) and high-resolution XPS spectra (Figure 3b) of boron-adsorbed resins enable near-surface elemental compositions of O, N, C, and B moieties to be determined. In a survey-scan XPS spectrum of boron-adsorbed resin, signals at 533, 399, 285, and 191 eV are attributed to the binding energies of O 1s, N 1s, C 1s, and B 1s electrons. Spectral deconvolution of these signals yields near-surface elemental compositions of O, N, C, and B atoms, which were 19, 3, 77, and 0.6 atom %, respectively. An O/N atom ratio of approximately 5.7 obtained from XPS measurements is consistent with the O/N ratio of 6.0 for A and B, according to their combined stoichiometry, indicating the presence of these NMDG-type moieties on the resin surfaces. While distinct binding energies associated with C and N atoms in high-resolution XPS spectra (Figure 3) suggest the presence of different carbon and nitrogen atom environments on the resin surface, direct assignments of binding energies to different nitrogen environments in alkyl amines or quaternary ammonium ions are infeasible, based on XPS analyses alone.

The different surface moieties A, B, C, and D on the NMDG-functionalized PSDVB resin can nevertheless be distinguished by their different nitrogen environments. Till now, this has been infeasible because of the low surface compositions of nitrogen and very low natural abundance and low gyromagnetic ratio of ^{15}N . However, recent advancements in surface-enhanced DNP-NMR enable these historical obstacles to be overcome. For boron-adsorbed resins, relatively high signal enhancements observed under DNP-NMR conditions allow different ^{15}N environments of dilute surface species (3 atom % N) at natural abundance ^{15}N (0.4%) to be detected, resolved and identified. For example, the solid-state $^{15}\text{N}\{^1\text{H}\}$ DNP-NMR spectrum (Figure 4) of a boron-adsorbed

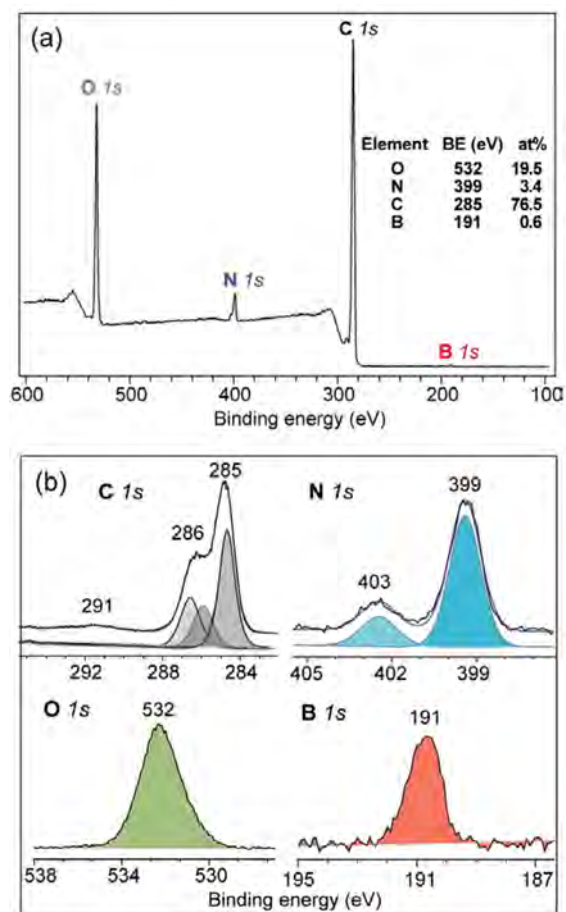


Figure 3. (a) Survey-scan and (b) high-resolution XPS spectra acquired at room temperature for a boron-adsorbed NMDG-functionalized PSDVB resin with binding energies (BE, eV) that correspond to C 1s, N 1s, O 1s, and B 1s electrons.

NMDG-functionalized PSDVB resin exhibited a well-resolved signal at 59 ppm and three partially resolved ^{15}N signals between 20 and 50 ppm. Deconvolution of the ^{15}N signals in the range 20–60 ppm suggests a distribution of isotropic ^{15}N chemical shifts with signals centered at approximately 29, 38, 45, and 59 ppm. First, to distinguish between different NMDG-type alkyl amines (Scheme 1), a separate $^{15}\text{N}\{^1\text{H}\}$ CP-MAS NMR spectrum for neat NMDG was acquired (Supporting Information, Figure S1), which exhibited a signal intensity at 25 ppm.⁶³ This indicates that the ^{15}N signal at 29 ppm of the functionalized resin likely originates from the tertiary amine group of A. The difference of 4 ppm between the isotropic ^{15}N chemical shifts of neat NMDG and the resin-grafted NMDG moieties is attributed to the variation of ^{15}N environments upon surface functionalization. The isotropic ^{15}N chemical shifts reported in the literature⁶⁴ suggest that ^{15}N signals associated with quaternary ammonium ions (here, B and D) are displaced to higher frequencies (i.e., higher ppm values) than those signals associated with the tertiary amines.⁶⁵ In addition, the ^{15}N chemical shifts of cyclic amines, such as C, are expected to appear at higher frequencies compared to linear alkyl amines, such as A.⁶⁴ Therefore, the ^{15}N signal intensity at 38 ppm is attributed to the tertiary amine moiety C. The remaining two signals at 45 and 59 ppm likely originate from the ^{15}N sites in quaternary ammonium ions in B and D moieties, respectively, which differ in their local bonding

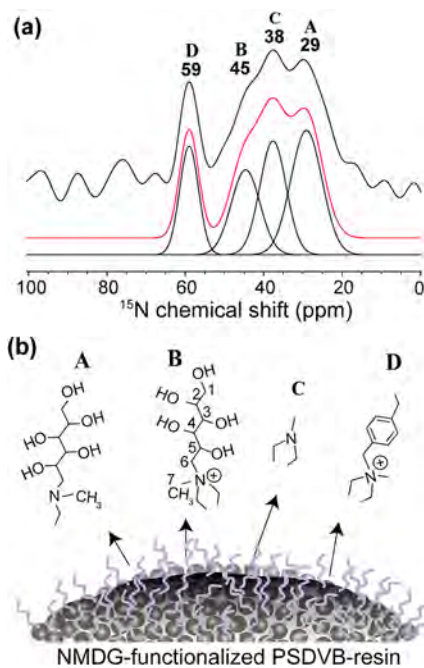


Figure 4. (a) Surface-enhanced 1D $^{15}\text{N}\{^1\text{H}\}$ DNP-MAS NMR spectrum of a boron-exposed NMDG-surface functionalized PSDVB resin on which ^{15}N signal assignments to A, B, C, and D moieties are based. The spectrum was acquired at 9.4 T, 92 K, and 8 kHz MAS and with a CP contact time of 2 ms using 16 mM TEKPol in 1,1,2,2-tetrachloroethane (b) Schematic diagram of the resin surface showing the different types of surface functional groups, A, B, C, and D.

environments. In particular, the higher frequency signal at 59 ppm is attributed to ^{15}N sites in cyclic quaternary ammonium ions, D, bearing an aromatic substituent and a positive charge, compared to the lower frequency signal at 45 ppm, consistent with ^{15}N sites in cyclic tertiary amine moieties, C. Although $^{15}\text{N}\{^1\text{H}\}$ CP-MAS signal intensities are not strictly quantitative, similarities in local $^{15}\text{N}\{^1\text{H}\}$ surface environments and low molecular mobilities at 92 K of the closely related A, B, C, and D moieties are expected to yield similar signal enhancements. Their comparable relative intensities suggest that these moieties are present in similar relative quantities and may influence boron adsorption properties of the resin.

Identification of Distinct Boron-Adsorption Sites. To understand the boron adsorption properties of the NMDG-functionalized PSDVB ion-exchange resins, it is important to identify and quantify boron adsorption sites on the resin surfaces. A previous study²⁵ hypothesized that borate anions adsorb on surface-grafted NMDG functional groups by forming chelate complexes. These could include bischelate complexes where borate anions interact with polyhydroxyl groups of neighboring NMDG moieties, monochelate complexes where borate anions coordinate to two hydroxyl groups within the same NMDG moiety, or tetradentate borate complexes where borate anions coordinate to four hydroxyl groups within the same NMDG moiety. Such chelate complexes are only expected to form when surface NMDG moieties bear hydroxyl groups. In contrast, surface functional groups without hydroxyl groups (e.g., the C and D moieties in Scheme 1) are expected to exhibit lower affinities to borate anions, which would likely occur mostly via weak interactions.

Distinct boron adsorption sites on the resin surfaces can nevertheless be distinguished and identified by using 1D ^{11}B

MAS NMR measurements. Such analyses are feasible even at relatively dilute quantities of borate anions, because of the high 80% natural abundance of ^{11}B . The 1D ^{11}B MAS NMR spectrum acquired at 11.7 T at room temperature (Figure 5a)

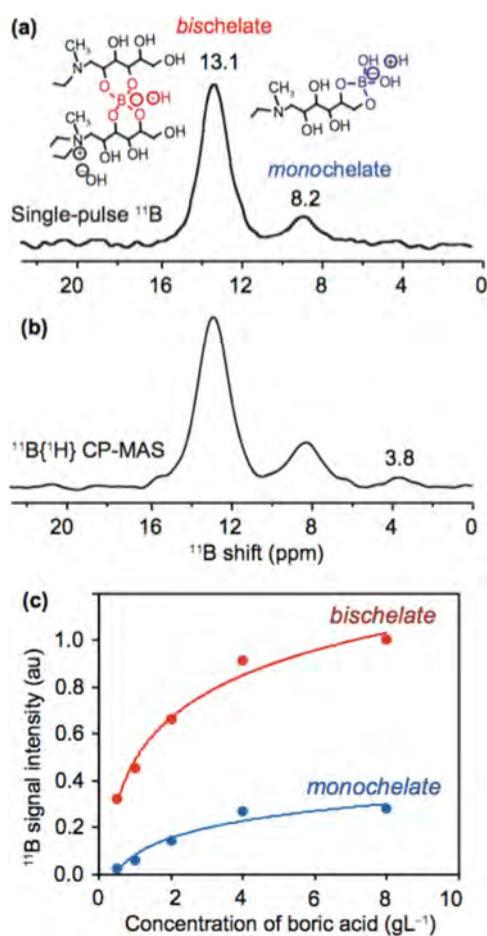


Figure 5. (a) Solid-state single-pulse 1D ^{11}B MAS NMR spectrum acquired at 11.7 T, 298 K, and 60 kHz MAS and (b) 1D $^{11}\text{B}\{^1\text{H}\}$ CP-MAS NMR spectrum acquired at 11.7 T, 298 K, and 8 kHz MAS of boron-adsorbed NMDG-resin. In (a), the integrals of signal intensities associated with the mono- vs bischelate complexes were found to be $17 \pm 3\%$ and $83 \pm 3\%$, respectively. (c) Plots of normalized $^{11}\text{B}\{^1\text{H}\}$ CP-signal intensity associated with the formation of mono- and bischelate complexes, as functions of boric acid concentration.

of a boron-exposed NMDG-functionalized PSDVB resin exhibited well-resolved ^{11}B signals at 13.1 and 8.2 ppm, which are attributed to distinct boron-adsorption sites on the resin surfaces. The positions and line shapes of the ^{11}B ($\text{spin } I = 3/2$) signals may be influenced by second-order quadrupolar interactions that are sensitive to the nature of bonding interactions and coordination number of the boron atoms. For example, tri- and tetraordinated boron atoms have been shown to exhibit different chemical shifts, line shapes, and quadrupole coupling constants,^{66–69} which permit such boron environments to be readily distinguished from each other. In particular, for the borate anions adsorbed on the NMDG-functionalized resin, the relatively narrow ^{11}B signal intensities (full-width-at-half-maximum of 200 Hz) and displacements of ^{11}B signals to lower frequencies (0–20 ppm) suggest the presence of tetrahedrally coordinated borate anions in chelate complexes.⁶⁶ Based on the ^{11}B signal assignments of

tetrahedrally coordinated borate anions in chelate complexes in the literature,^{24,70,71} the ^{11}B intensities at 8.2 and 13.1 ppm in Figure 5a are assigned to borate anions in mono- and bischelate complexes, respectively.

To gain quantitative insight into the relative populations of the different adsorbed boron species, the integrated ^{11}B signals associated with the mono- (8.2 ppm) versus the bischelate (13.1 ppm) were measured and compared. Based on their integrated ^{11}B intensities in the single-pulse ^{11}B MAS NMR spectrum of Figure 5a, the relative percentages of borate anions adsorbed as mono- or bischelate complexes were determined to be $17 \pm 3\%$ and $83 \pm 3\%$, respectively. This points to preferential formation of bischelated borate anion complexes, compared to monochelated boron species, on the NMDG-functionalized PSDVB resin surfaces.

The molecular-level origins that account for selective boron adsorption as bischelate complexes have been challenging to establish. It has been hypothesized that the borate anions electrostatically interact with the residual metal cations present on the NMDG-functionalized resin surface.²⁴ For the NMDG-functionalized PSDVB-resin, ICP atomic emission spectroscopy analyses showed that trace amounts of metal cations were present, although their absolute and relative quantities were small (Supporting Information, Table S1). While borate anions could interact with traces of such metal cations, no such additional signals are detected in the single-pulse 1D ^{11}B MAS NMR spectrum of Figure 5a (within the sensitivity limits of the measurement). Nevertheless, an additional signal is observed at 3.8 ppm in the 1D $^{11}\text{B}\{^1\text{H}\}$ CP-MAS spectrum of Figure 5b. The excitation of abundant ^1H nuclei and subsequent polarization transfer via ^1H – ^{11}B dipole–dipole interactions to nearby (<1 nm) ^{11}B nuclei enhances the intensity of this weak ^{11}B signal at 3.8 ppm, which is attributed to borate–metal complexes, consistent with previous observations in the literature.²⁴ These relatively weakly interacting borate anions can be desorbed and removed from the resin surface by subsequent washing (Supporting Information, Figure S2), after which no detectable signal at 3.8 ppm remains, while $^{11}\text{B}\{^1\text{H}\}$ CP-MAS signals from the boron chelate complexes at 8.2 and 13.1 ppm persist.

The adsorption behaviors of borate anions on the NMDG-functionalized resins can be understood by titrating initially boron-free resin surfaces with aqueous solutions containing different concentrations of borate anions. A plot of the integrated ^{11}B signal intensities of surface-adsorbed borate anions in mono- and bischelate complexes, as measured in 1D $^{11}\text{B}\{^1\text{H}\}$ CP-MAS spectra as a function of boric acid concentration (Figure 5c), shows an increasing trend in boron uptake as the boric acid concentration increased from 0.5 to 8 g L^{-1} . Although the ^{11}B intensities associated with mono- and the bischelate complexes are enhanced by cross-polarization from nearby protons and thus are not strictly quantitative, the local boron bonding environments are expected to yield similar signal enhancements and provide a reasonable estimate for the relative percentages of borate anions in mono- versus bischelate complexes. In particular, the $^{11}\text{B}\{^1\text{H}\}$ CP-MAS signal intensities from the bischelate complexes are significantly higher than those for the monochelate complexes and similar to the relative integrated intensities of the same signals in the single-pulse ^{11}B MAS spectrum of Figure 5a. Moreover, the relative intensities were similar over the range of boric acid concentrations investigated (0.5–8 g L^{-1}), which suggests that the

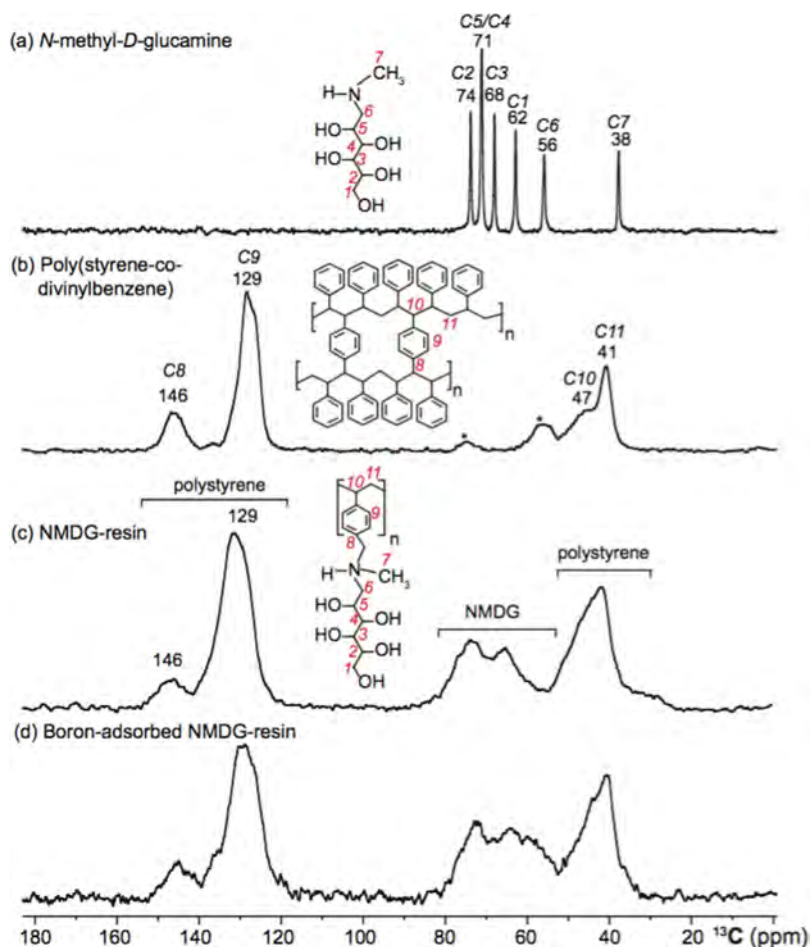


Figure 6. Solid-state $1\text{D } ^{13}\text{C}\{^1\text{H}\}$ CP-MAS NMR spectra acquired at 11.7 T, 298 K, and 8 kHz MAS of (a) NMDG (b) the PSDVB resin, and (c,d) the NMDG-functionalized PSDVB resin (c) before and (d) after exposure to boron. Asterisks denote spinning side bands.

concentration of borate anions in aqueous solution does not have a large influence on the selectivity of boron adsorption for bischolate complexes on the resin surfaces. It is noteworthy that a similar trend was observed for boron-adsorbed anion exchange resins and guanosine borate hydrogels,^{24,70,71} where the formation of borate diesters was preferred over the formation of monoesters to facilitate gelation. The $1\text{D } ^{11}\text{B}$ MAS and $^{11}\text{B}\{^1\text{H}\}$ CP-MAS NMR measurements thus allow the different distributions of boron adsorption species on the resin surface to be resolved and their relative populations to be estimated, although they provide little information on the specific interactions between borate anions and the surface functional groups.

Interactions between Borate Anions and Surface Functional Groups. Analyses of the intermolecular interactions that account for the formation of chelate complexes are expected to aid understanding of their roles and influences on macroscopic boron adsorption properties. Local structures of boron chelate complexes and their mutual interactions can be established by analyzing solid-state ^1H , ^{13}C and ^{11}B MAS NMR spectra, although severely overlapped ^1H and ^{13}C signals often hinder such analyses. For example, separate $1\text{D } ^1\text{H}$ and ^{13}C MAS NMR spectra of NMDG, the PSDVB resin, and the NMDG-functionalized PSDVB resin were acquired and compared. All show broad distributions of ^1H intensities between 0 and 10 ppm (Supporting Information, Figure S3), which were not feasible to assign to specific sites. Improved

resolution was obtained in the $1\text{D } ^{13}\text{C}\{^1\text{H}\}$ CP-MAS NMR spectra (Figure 6), which enabled assignments of the following ^{13}C signals: $-\text{NCH}_3$ (C7, 38 ppm), $-\text{NCH}_2$ (C6, 56 ppm), and $-\text{CH}$ (C5, C4, C3, and C2 at 71, 68, and 74 ppm, respectively) and $-\text{CH}_2$ (C1, 62 ppm) groups of NMDG moieties (Figure 6a).²⁴ In a similar manner, the analysis of the $1\text{D } ^{13}\text{C}\{^1\text{H}\}$ CP-MAS NMR spectrum of PSDVB resin enabled the assignments of the methylene (CH_2 , 41 ppm), benzylic (CH , 47 ppm), and aromatic (127, 129, and 146 ppm) ^{13}C moieties of PSDVB resin (Figure 6b), and their similar spectral features in the $^{13}\text{C}\{^1\text{H}\}$ CP-MAS NMR spectrum of NMDG-functionalized resin (Figure 6c).

By comparison, the $1\text{D } ^{13}\text{C}\{^1\text{H}\}$ CP-MAS NMR spectra of NMDG-functionalized resins (Figure 6c,d) before and after exposure to boron showed different distributions of ^{13}C isotropic chemical shifts associated with the NMDG surface moieties. For example, Figure 6c shows the solid-state 1D single-pulse ^{13}C MAS spectrum of the NMDG-functionalized PSDVB resin, where ^{13}C signals are observed from phenylene (146 and 135–125 ppm) and vinyl (47, 41 ppm) groups of PSDVB and from the alkyl groups (50–80 ppm) of NMDG. Compared to the spectrum of NMDG alone (Figure 6a), broad and nearly featureless ^{13}C signals are observed in the region 50–80 ppm, which reflects the compositional and structural heterogeneity of the NMDG-functionalized resin. While the ^{13}C signal intensities associated with PSDVB and NMDG surface moieties can be distinguished in Figure 6d,

subtle differences in the distributions of the ^{13}C chemical shifts in the region 50–80 ppm could be attributed to the changes in the ^{13}C environments of the NMDG surface moieties A and B upon exposure to boron.

The different NMDG functional moieties A, B, C, and D on the PSDVB resin surface are shown schematically in Figure 7a,

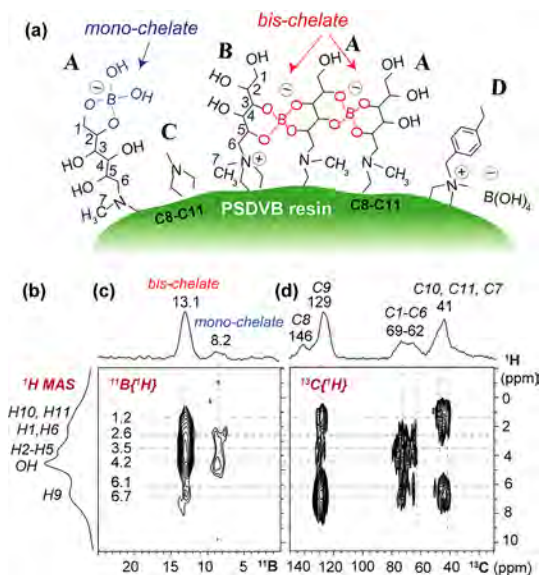


Figure 7. (a) Schematic diagram of the PSDVB resin surface consisting of tertiary amines (A, C) and quaternary ammonium ions (B, D), some of which are cross-linked by borate mono- and bischelate complexes. Solid-state NMR spectra of the boron-adsorbed NMDG-functionalized resin acquired at 11.7 T and at room temperature; (b) single-pulse ^1H NMR spectrum acquired at 60 kHz MAS and (c) $2\text{D } ^{13}\text{C}\{^1\text{H}\}$ and (d) $2\text{D } ^{11}\text{B}\{^1\text{H}\}$ HETCOR NMR spectra acquired at 12.5 kHz MAS each by using CP contact time of 2 ms, plotted with $1\text{D } ^{13}\text{C}\{^1\text{H}\}$ and $^{11}\text{B}\{^1\text{H}\}$ CP-MAS spectra on the top horizontal dimensions, respectively.

the structures of which are consistent with the 2D NMR analyses in Figure 7b–d. A combination of solid-state $2\text{D } ^{11}\text{B}\{^1\text{H}\}$ and $^{13}\text{C}\{^1\text{H}\}$ heteronuclear correlation (HETCOR) NMR spectra enables the molecular interactions between adsorbed borate anions and NMDG functional groups to be unambiguously identified. Such spectra are sensitive to heteronuclear dipole–dipole interactions between ^{11}B and ^1H nuclei or between ^{13}C and ^1H nuclei, which permit the chemical shifts of coupled spin pairs to be correlated. Enhanced resolution provided by the $2\text{D } ^{11}\text{B}\{^1\text{H}\}$ HETCOR spectrum, in which intensity correlations from multiple ^1H signals are resolved in the vertical ^1H dimension, can be distinguished at 2.6 and 3.5 ppm for the $-\text{NCH}_2$ and $-\text{CH}$ moieties of NMDG, and 6.7 ppm for the aromatic groups of PSDVB. Strong 2D intensity correlations are observed between the ^{11}B signal at 13.1 ppm associated with bischelated borate anions and the ^1H signals at 2.6 and 3.5 ppm, which are thus assignable to different $-\text{CH}$ and $-\text{CH}_2$ groups of the NMDG moieties, respectively. These correlated intensities indicate that the borate anions in the bischelate complexes interact with the hydroxyl groups of C2–C5 of NMDG moieties, as depicted in the schematic diagram in Figure 7a. Two weaker intensity correlations are observed between the ^{11}B signal at 8.2 ppm associated with monochelated borate anions and ^1H signals at approximately 2.6 and 4.2 ppm that likely correspond to the

terminal $-\text{CH}_2$ and terminal $-\text{OH}$ groups of the C1 and C2 NMDG moieties, which suggests that these borate anions interact with the NMDG end groups (Figure 7a). Although the ^1H resolution is limited, the ^1H and ^{11}B signals associated with different boron adsorption sites can be resolved by correlating their respective signals in the 2D frequency map. Such strong correlated intensities are expected to originate principally from borate anions that are cross-linked to hydroxyl groups of adjacent NMDG functional groups, consistent with the formation of chelate complexes on the PSDVB resin surface.^{24,70,71} The absence of correlated ^{11}B (~ 3.8 ppm) and ^1H signals rules out the possibility of a significant fraction of weakly adsorbed borate anions on the NMDG-functionalized resin surface.

Complementary insights on the local structures of the chelate complexes can be obtained by analyzing the $2\text{D } ^{13}\text{C}\{^1\text{H}\}$ HETCOR spectrum of boron-adsorbed NMDG-functionalized PSDVB resin (Figure 7d), which correlates the isotropic ^1H and ^{13}C chemical shifts of dipole–dipole-coupled spin pairs. As for the $2\text{D } ^{11}\text{B}\{^1\text{H}\}$ HETCOR spectrum, severely overlapping ^1H signals are resolved in the indirect (vertical) dimension of the spectrum, which allows the ^1H signals to be confidently assigned to $-\text{NCH}_3$, $-\text{NCH}_2$, $-\text{CH}_2$, $-\text{CH}$, $-\text{NH}$, and aromatic groups through their ^{13}C – ^1H intensity correlations. The assignments of ^{13}C signals are based on the analyses of 1D and $2\text{D } ^{13}\text{C}\{^1\text{H}\}$ CP-MAS and HETCOR spectra of NMDG, PSDVB resin, and NMDG-functionalized resin shown in Figure 7 and in the Supporting Information, Figures S4–S7. Based on analyses of the latter, strong intensity correlations associated with dipole–dipole-coupled ^{13}C – ^1H moieties in the $2\text{D } ^{13}\text{C}\{^1\text{H}\}$ HETCOR spectrum of the boron-adsorbed resin (Figure 7d) were distinguished and identified: ^{13}C NMR signals at 40–45 ppm (C10, C11) and ^1H NMR signals at 1.2–2.2 ppm (H10, H11) originate from the vinyl groups and ^{13}C signals in the range 125–135 ppm (C9) and ^1H signals at 6.7 ppm are associated with aromatic groups of the PSDVB resin, respectively. Likewise, a broad distribution of correlated $2\text{D } ^{13}\text{C}$ signal intensities in the range 60–75 ppm (C1–C6) and ^1H signals in the range 2.2–4.2 (H1–H6) ppm is attributed to the directly bonded ^{13}C – ^1H pairs in the of the surface-grafted NMDG groups on the PSDVB resin.

Of particular interest are the distributions of correlated $2\text{D } ^{13}\text{C}$ signals in the range of 60–75 ppm and ^1H signals at 6.7 ppm, and between ^{13}C signals at 125–135 ppm and ^1H signals at 2.2–4.2 ppm, which indicate the sub-nanometer proximities (<1 nm) between the NMDG surface functional groups and the PSDVB resin. In addition, spatial proximity between $-\text{NH}$ sites of NMDG and aromatic groups of PSDVB is manifested by strong 2D intensity correlations between ^{13}C signals 60–75 ppm (C1–C6) in Figure 7d and ^1H signals at 6.1 ppm in Figures 7c,d, which establish the nanoscale proximities of the adsorbed borate anions in bischelate complexes (^{11}B , 13.1 ppm), $-\text{NH}$ groups of NMDG, and the PSDVB resin. In contrast, the absence of such as correlated signals between ^{11}B and ^1H suggests that borate anions in the monochelate complexes are adsorbed near the end groups (C1 and C2) of surface NMDG moieties, as depicted in the schematic diagram (Figure 7a). This is further supported by the presence of a strong correlated signal intensity between the borate anions in monochelate complexes (^{11}B , 8.2 ppm) and hydroxyl groups ($-\text{OH}$, 4.2 ppm). Importantly, the different chelate complexes and the assignments of their associated ^1H , ^{11}B , and ^{13}C

chemical shifts enable the interactions between the borate anions and different adsorption sites to be probed by complementary solid-state $2D\ ^{11}B\{^1H\}$ and $^{13}C\{^1H\}$ HETCOR NMR measurements.

The solid-state NMR results were corroborated by FT-IR analyses (Figure 8) that showed distinct spectral features for

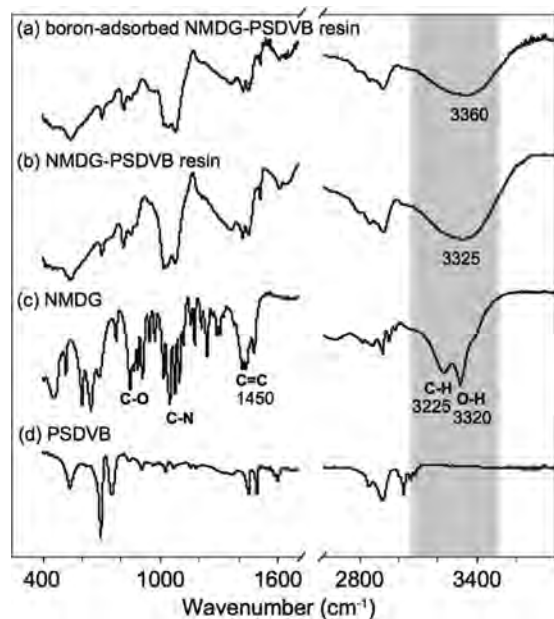


Figure 8. Solid-state FT-IR spectra acquired at room temperature of the NMDG-functionalized PSDVB-resin (a) after and (b) before exposure to boron, (c) NMDG, and (d) PSDVB-resin. Vibrational stretching frequencies associated with C–O, C–N, C=C, C–H, N–H, and O–H bonds of the different local bonding environments of the mono- and bischelate complexes are shown. The vertical shaded region depicts subtle changes associated with the C–H and –OH vibrational frequencies upon boron exposure.

NMDG, PSDVB-resin and NMDG-functionalized PSDVB-resins before and after exposure to boron. Broad distributions of signals in the ranges of $1000\text{--}1200\text{ cm}^{-1}$ and $3100\text{--}3500\text{ cm}^{-1}$ (gray shaded region) in the FT-IR spectra of NMDG-functionalized PSDVB-resins manifest the heterogeneity of the resin surfaces. By comparison, relatively narrow signals are observed for the NMDG functional groups. In particular, a displacement of C–H (3225 cm^{-1}) and O–H (3320 cm^{-1}) bonding vibrational frequencies (Figure 7b) to higher values of 3325 cm^{-1} (Figure 7c) indicate changes in the local C–H and O–H bonding environments upon surface-grafting of the NMDG moieties (Figure 8c). In addition, further displacement of $\sim 35\text{ cm}^{-1}$ in the vibrational bands toward higher frequency (3360 cm^{-1}) in the FT-IR spectrum of boron-adsorbed resins (Figure 8b) reflects changes in local bonding environments of the tertiary amines, quaternary ammonium ions, and hydroxyl groups in chelate complexes upon boron exposure.

Proximities of Adsorbed Borate Anions on the Resin Surface. The $1D\ ^{11}B$ MAS and $2D\ ^{11}B\{^1H\}$ CP-MAS NMR analyses above provide valuable information on distinct boron adsorption sites, relative populations of adsorbed borate anions, and local structures of borate anions in mono- and bischelate complexes. However, they provide limited information on the distributions of the chelated borate anion complexes on the NMDG-functionalized resin surfaces. Complementary insights into the local structures of borate-

chelate complexes were obtained by analyzing a $2D\ ^{11}B\{^{11}B\}$ homonuclear dipolar-mediated spectrum. Spatially proximate borate complexes ($<1\text{ nm}$) are expected to manifest correlated signal intensities in $2D\ ^{11}B\{^{11}B\}$ dipolar correlation NMR spectra acquired at different spin-diffusion mixing times, which are characteristic of the strengths of $^{11}B\text{--}^{11}B$ dipole–dipole interactions. The feasibility of observing such $2D$ correlation intensities can, however, be realized only when two or more borate anions are adsorbed to the same NMDG moiety or to adjacent NMDG moieties grafted onto the resin surfaces. For example, the $2D\ ^{11}B\{^{11}B\}$ spectrum in Figure 9 acquired using

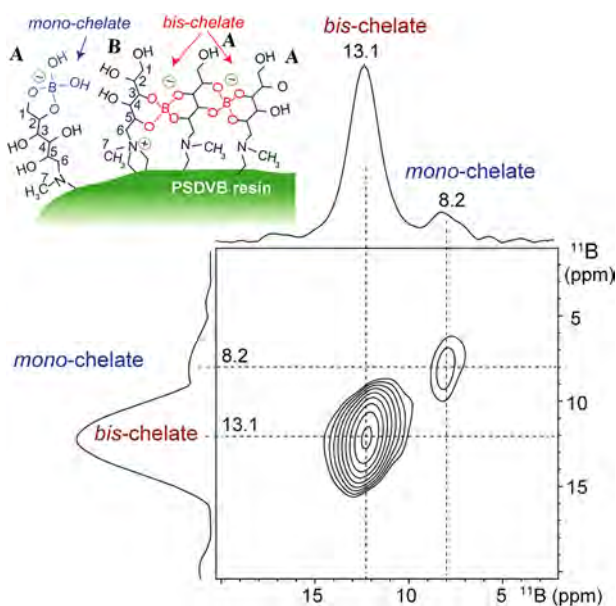


Figure 9. Solid-state $2D\ ^{11}B\{^{11}B\}$ dipolar correlation NMR spectrum of boron adsorbed on NMDG-functionalized PSDVB resin; the spectrum was acquired 20 T (850 MHz for 1H), 298 K, and 25 kHz MAS. The diagonal intensity correlations at 8.2 and 13.1 ppm correspond to ^{11}B signals of borate anions adsorbed on mono- and bischelate sites of the NMDG-functionalized resin surface, as depicted in the schematic structures in the inset.

a short spin-diffusion mixing time of 100 ms exhibits diagonal intensity correlations that correspond to ^{11}B signals that are associated with isolated populations of mono- and bischelate complexes on the NMDG-functionalized resin surface. No off-diagonal intensity correlations are observed between the ^{11}B signals of borate anions adsorbed in mono- (8.2 ppm) and bischelate (13.1 ppm) complexes, even for longer spin-diffusion times of up to 1 s. The solid-state $^{11}B\{^{11}B\}$ results are consistent with the oxygen-to-boron ratio 35 atom % measured from XPS analysis of the boron-adsorbed resin (Figure 3). Combined solid-state NMR and XPS analyses suggest that the borate anions are sparsely distributed on the resin surface and that the adsorbed mono- and bischelate boron sites appear to be at least 1 nm apart or farther.

Correlating Surface Compositions and Structures with Boron Adsorption Properties. The molecular interactions that account for different boron adsorption properties are related to the nanoscale surface compositions and structures of the NMDG functional groups and their byproducts. NMDG-functionalized PSDVB resins synthesized under different conditions exhibited subtle differences in their adsorption behaviors upon exposure to borate anions in

aqueous solutions, which are expected to originate from different surface compositions. This is corroborated by the measurement of total ion-exchange capacities (TEC, A + B + C) by ion titration methods for two different resin preparations, which we refer to here as batches I and II. To better understand the different factors that ultimately influence the boron-adsorption properties of different NMDG-resin batches, combined XPS and solid-state NMR (Supporting Information, sections 5–8) analyses were carried out. For both resin batches, near-surface concentrations of O, N, C and B atoms were measured by the deconvolution of XPS signal intensities at 532, 399, 285, and 191 eV associated with the binding energies of O 1s, N 1s, C 1s, and B 1s electrons, respectively (Supporting Information, Figure S8). Subtle differences in the oxygen-to-boron (O/B) ratios of 39 and 33, nitrogen-to-boron (N/B) ratios of 7.2 and 6.2, and oxygen-to-nitrogen (O/N) ratios of 5.4 and 5.7 in batch I and II resins (Table 2) suggest different surface compositions of A, B, and C (and D) exchange sites on the NMDG-functionalized resins (Supporting Information, Table S3).

Table 2. Surface Elemental Compositions and Boron Adsorption Capacities of Different Resin Batches

	batch I	batch II
O/B ratio (atom %) ^a	39	32.5
N/B ratio (atom %) ^a	7.2	6.2
O/N ratio (atom %) ^a	5.4	5.7
boron concn (ppm) ^b	2500	2500
total exchange capacity (A + B + C + D) (mmol/g) ^c	2.7	3.2

^aDetermined from XPS analyses. ^bDetermined from ICP-MS elemental analysis. ^cDetermined from titration experiments.

A more insightful distinction of the atomic-level structures results from surface-enhanced ¹⁵N{¹H} DNP-MAS NMR spectra, which show different distributions of ¹⁵N signal intensities (Supporting Information, Figure S9). Deconvolution of the ¹⁵N{¹H} signals enabled distinct ¹⁵N environments on the resin surfaces to be identified. For the batch I resin, ¹⁵N signals at 59, 45, 38, and 29 ppm are assigned to ¹⁵N environments in D, B, C, and A, respectively, as discussed above. Similarly, for the batch II resin, ¹⁵N signals at 46, 38, and 29 ppm are assigned to ¹⁵N environments in B, C and A, respectively, with little or no signal intensity observed at 59 ppm. Although ¹⁵N{¹H} DNP-MAS NMR spectra are not necessarily quantitative, an estimation of the relative quantities of A, B, C, and D exchange sites in the batch I and II resins can be obtained by deconvoluting of ¹⁵N signal intensities (Supporting Information, Table S4). This leads to estimates for the relative densities of NMDG-type A and B exchange sites containing hydroxyl groups that account for boron adsorption of 34 + 22 = 56 (±5%) for the batch I resin and 22 + 46 = 68 (±5%) for the batch II resin. The different boron adsorption properties of the different resins likely result from their synthesis and processing conditions, which lead to distinct resin surface compositions. Combined XPS and surface-enhanced 1D ¹⁵N{¹H} DNP MAS NMR analyses suggest that the batch II resin has a relatively higher concentration of B exchange sites that leads to improved adsorption properties compared to the batch I resin. In spite of the relative differences in the surface compositions, the concentrations of borate anions adsorbed on batch I and II

resins were determined by ICP-MS analyses to both be approximately 2500 ppm (Table 2).

The boron adsorption behaviors of different resin batches were assessed by analyzing solid-state 1D ¹¹B{¹H} CP-MAS NMR spectra of boron-free resins titrated with different concentrations of borate anions (Supporting Information, Figure S10). The analyses of boron adsorption isotherms determined from the 1D ¹¹B{¹H} signal intensities associated with the mono- (8.2 ppm) and bischelate (13.1 ppm) complexes (Figure S10) showed subtle differences for the different resins. In particular, the batch II resin exhibited superior boron adsorption behavior than the batch I resin, which reflects their different distributions of A and B anion-exchange sites. In particular, NMDG-type B surface moieties consisting of quaternary ammonium cations are expected to electrostatically interact with borate anions and form cross-links with polyhydroxyl groups, consistent with their enhanced binding affinities, compared to A sites on the resin surfaces. The enhanced performance of batch II resin thus appears to be associated with a higher concentration of B exchange sites. Although different local compositions tend to influence the total boron adsorption properties, the mechanism of boron adsorption is expected to involve the formation of stable chelate complexes in both resin batches. This is further corroborated by analyses 2D ¹¹B{¹H} and ¹³C{¹H} HETCOR NMR spectra (Supporting Information, Figure S11) for the batch I and II resins, which exhibit similar correlated signals and intensities that point to similar interactions between the adsorbed borate anions and hydroxyl groups of the NMDG functional groups.

CONCLUSIONS

To summarize, the nanoscale surface compositions and structures that account for different boron-adsorption properties of anion-exchange resins have been unknown until now because of the dilute concentrations (3 atom %) of surface moieties and low isotopic natural abundances of NMR-active species (e.g., ¹⁵N, 0.4%). An atomic-level understanding of reactive polymer surfaces and interfaces that lack long-range structural order is difficult to establish by using conventional techniques, such as X-ray diffraction, XPS, or electron microscopy. Boron-adsorbed resin surfaces bearing different types of NMDG surface moieties have been characterized by combining XPS and DNP-enhanced ¹⁵N MAS NMR spectroscopy and conventional solid-state ¹H, ¹¹B, and ¹³C solid-state NMR. The sensitivity and resolution associated with NMR spectroscopy, especially 2D and DNP methods, permit subtly different moieties to be identified and distinguished at distinct boron adsorption sites on heterogeneous polymer surfaces. In particular, surface-enhanced ¹⁵N DNP-NMR spectra enabled different ¹⁵N local environments in tertiary amines and quaternary ammonium ions to be detected, identified, and quantified. The surface-enhanced DNP-NMR results were corroborated by XPS analyses, which showed different near-surface elemental compositions of O, C, N, and B atoms. In addition, ¹¹B MAS NMR analyses revealed approximately 83 ± 3% of borate anions were adsorbed on the resin surface in the form of bischelate complexes and 17 ± 3% as monochelate complexes. Local structures of chelate complexes were established by analyzing 2D ¹¹B{¹H} and ¹³C{¹H} HETCOR NMR spectra of NMDG, PSDVB, and boron-adsorbed resin, which established that the surface-adsorbed borate anions are in close proximity to the hydroxyl groups of the NMDG

moieties. The use of solid-state DNP-enhanced NMR spectroscopy, together with FT-IR and macroscopic analyses, represents a general approach toward measuring, correlating, and quantifying nanoscale surface compositions and structures with the adsorption properties of diverse functionalized resins. The resulting molecular-level understanding of compositions, densities, and distributions of ion-exchange sites is expected to guide rational design of resins with improved adsorption properties for applications in environmental remediation, separation and purification, and catalysis, the functional properties of which depend strongly on surface compositions and structures.

■ ASSOCIATED CONTENT

Supporting Information

The Supporting Information is available free of charge on the ACS Publications website at DOI: 10.1021/acs.langmuir.9b02042.

Surface-enhanced 1D $^{15}\text{N}\{^1\text{H}\}$ DNP-MAS NMR spectra; elemental concentrations of metal ions in NMDG-functionalized resins; solid-state 1D $^{11}\text{B}\{^1\text{H}\}$ CP-MAS NMR spectra; solid-state 1D ^1H MAS NMR spectra; 2D $^{13}\text{C}\{^1\text{H}\}$ HETCOR NMR spectra; solid-state 2D $^1\text{H}\{^1\text{H}\}$ DQ-SQ NMR correlation spectra; experimental ^1H SQ and DQ chemical shifts; XPS analyses and survey scan spectra; deconvoluted signal integrals and line shape analyses (PDF)

■ AUTHOR INFORMATION

ORCID

G. N. Manjunatha Reddy: 0000-0002-8283-2462

Bradley F. Chmelka: 0000-0002-4450-6949

Notes

The authors declare no competing financial interest.

■ ACKNOWLEDGMENTS

Financial support from Mitsubishi Chemical–Center for Advanced Materials (MC-CAM) is gratefully acknowledged. Surface-enhanced DNP NMR, conventional solution- and solid-state NMR, SEM, X-ray diffraction, XPS, ICP-MS tracer analysis, and FT-IR experiments were conducted using the Shared Facilities of the UCSB Materials Research Laboratory supported by the MRSEC program of the U.S. NSF under Award No. DMR-1720256, a member of the NSF-funded Materials Research Facilities Network (www.mrfn.org).

■ REFERENCES

- (1) Zuo, K. C.; Cai, J. X.; Liang, S.; Wu, S. J.; Zhang, C. Y.; Liang, P.; Huang, X. A Ten Liter Stacked Microbial Desalination Cell Packed With Mixed Ion-Exchange Resins for Secondary Effluent Desalination. *Environ. Sci. Technol.* **2014**, *48*, 9917–9924.
- (2) Jacob, C. Seawater Desalination: Boron Removal by Ion Exchange Technology. *Desalination* **2007**, *205*, 47–52.
- (3) Hanke, A. T.; Ottens, M. Purifying Biopharmaceuticals: Knowledge-Based Chromatographic Process Development. *Trends Biotechnol.* **2014**, *32*, 210–220.
- (4) Gelbard, G. Organic Synthesis by Catalysis with Ion-Exchange Resins. *Ind. Eng. Chem. Res.* **2005**, *44*, 8468–8498.
- (5) Feng, Y.; He, B.; Cao, Y.; Li, J.; Liu, M.; Yan, F.; Liang, X. Biodiesel Production Using Cation-Exchange Resin as Heterogeneous Catalyst. *Bioresour. Technol.* **2010**, *101*, 1518–1521.
- (6) Shibasaki-Kitakawa, N.; Hiromori, K.; Ihara, T.; Nakashima, K.; Yonemoto, T. Production of High Quality Biodiesel from Waste Acid

Oil Obtained during Edible Oil Refining Using Ion-Exchange Resin Catalysts. *Fuel* **2015**, *139*, 11–17.

(7) Nishihama, S.; Sumiyoshi, Y.; Ookubo, T.; Yoshizuka, K. Adsorption of Boron Using Glucamine-Based Chelate Adsorbents. *Desalination* **2013**, *310*, 81–86.

(8) Guan, Z.; Lv, J.; Bai, P.; Guo, X. Boron Removal from Aqueous Solutions by Adsorption – A Review. *Desalination* **2016**, *383*, 29–37.

(9) Wang, L.; Qi, T.; Gao, Z.; Zhang, Y.; Chu, J. Synthesis of N-Methylglucamine Modified Macroporous Poly(GMA-co-TRIM) and Its Performance as a Boron Sorbent. *React. Funct. Polym.* **2007**, *67*, 202–209.

(10) Biçak, N.; Şenkal, B. F. Sorbitol-Modified Poly(N-Glycidyl Styrene Sulfonamide) for Removal of Boron. *J. Appl. Polym. Sci.* **1998**, *68*, 2113–2119.

(11) Tu, K. L.; Chivas, A. R.; Nghiem, L. D. Enhanced Boron Rejection by NF/RO membranes by Complexation with Polyols: Measurement and Mechanisms. *Desalination* **2013**, *310*, 115–121.

(12) Recepoglu, Y. K.; Kabay, N.; Yilmaz-Ipek, I.; Arda, M.; Yuksel, M.; Yoshizuka, K.; Nishihama, S. Deboronation of Geothermal Water Using N-methyl-D-Glucamine Based Chelating Resins and a Novel Fiber Adsorbent: Batch and Column Studies. *J. Chem. Technol. Biotechnol.* **2017**, *92*, 1540–1547.

(13) Qian, P.; Schoenau, J. J. Practical Applications of Ion Exchange Resins in Agricultural and Environmental Soil Research. *Can. J. Soil Sci.* **2002**, *82*, 9–21.

(14) Guzman, I.; Heras, A.; Guemez, M. B.; Iriondo, A.; Cambra, J. F.; Requies, J. Levulinic Acid Production Using Solid-Acid Catalysis. *Ind. Eng. Chem. Res.* **2016**, *55*, 5139–5144.

(15) Harmer, M. A.; Sun, Q. Solid Acid Catalysis Using Ion-Exchange Resins. *Appl. Catal., A* **2001**, *221*, 45–62.

(16) Kiss, A. A.; Dimian, A. C.; Rothenberg, G. Solid Acid Catalysts for Biodiesel Production - Towards Sustainable Energy. *Adv. Synth. Catal.* **2006**, *348*, 75–81.

(17) Gomes, H. I.; Jones, A.; Rogerson, M.; Greenway, G. M.; Lisbona, D. F.; Burke, I. T.; Mayes, W. M. Removal and Recovery of Vanadium from Alkaline Steel Slag Leachates with Anion Exchange Resins. *J. Environ. Manage.* **2017**, *187*, 384–392.

(18) Bertagnolli, C.; Grishin, A.; Vincent, T.; Guibal, E. Boron Removal by a Composite Sorbent: Polyethylenimine/Tannic Acid Derivative Immobilized in Alginate Hydrogel Beads. *J. Environ. Sci. Health, Part A: Toxic/Hazard. Subst. Environ. Eng.* **2017**, *52*, 359–367.

(19) Suri, A. K.; Subramanian, C.; Sonber, J. K.; Murthy, T. S. R. C. Synthesis and Consolidation of Boron Carbide: a Review. *Int. Mater. Rev.* **2010**, *55*, 4–40.

(20) Tang, Y. P.; Luo, L.; Thong, Z. W.; Chung, T. S. Recent Advances in Membrane Materials and Technologies for Boron Removal. *J. Membr. Sci.* **2017**, *541*, 434–446.

(21) Weng, Q.; Wang, X.; Wang, X.; Bando, Y.; Golberg, D. Functionalized Hexagonal Boron Nitride Nanomaterials: Emerging Properties and Applications. *Chem. Soc. Rev.* **2016**, *45*, 3989–4012.

(22) Venegas, J. M.; McDermott, W. P.; Hermans, I. Serendipity in Catalysis Research: Boron-Based Materials for Alkane Oxidative Dehydrogenation. *Acc. Chem. Res.* **2018**, *51*, 2556–2564.

(23) Schlienger, S.; Alauzun, J.; Michaux, F.; Vidal, L.; Parmentier, J.; Gervais, C.; Babonneau, F.; Bernard, S.; Miele, P.; Parra, J. B. Micro-, Mesoporous Boron Nitride-Based Materials Templated from Zeolites. *Chem. Mater.* **2012**, *24*, 88–96.

(24) Sasaki, K.; Qiu, X.; Miyawaki, J.; Ideta, K.; Takamori, H.; Moriyama, S.; Hirajima, T. Contribution of Boron-Specific Resins Containing N-Methylglucamine Groups to Immobilization of Borate/Boric Acid in a Permeable Reactive Barrier Comprising Agglomerated MgO. *Desalination* **2014**, *337*, 109–116.

(25) Yoshimura, K.; Miyazaki, Y.; Ota, F.; Matsuoka, S.; Sakashita, H. Complexation of Boric Acid with the N-Methyl-D-Glucamine group in Solution and in Crosslinked Polymer. *J. Chem. Soc., Faraday Trans.* **1998**, *94*, 683–689.

(26) Karahan, S.; Yurdakoç, M.; Seki, Y.; Yurdakoç, K. Removal of Boron from Aqueous Solution by Clays and Modified Clays. *J. Colloid Interface Sci.* **2006**, *293*, 36–42.

- (27) Bernstein, R.; Belfer, S.; Freger, V. Toward Improved Boron Removal in RO by Membrane Modification: Feasibility and Challenges. *Environ. Sci. Technol.* **2011**, *45*, 3613–3620.
- (28) Cengeloglu, Y.; Arslan, G.; Tor, A.; Kocak, I.; Dursun, N. Removal of Boron from Water by using Reverse Osmosis. *Sep. Purif. Technol.* **2008**, *64*, 141–146.
- (29) Kabay, N.; Arar, O.; Acar, F.; Ghazal, A.; Yuksel, U.; Yuksel, M. Removal of Boron from Water by Electrodialysis: Effect of Feed Characteristics and Interfering Ions. *Desalination* **2008**, *223*, 63–72.
- (30) Wolska, J.; Bryjak, M. Preparation of Polymeric Microspheres for Removal of Boron by Means of Sorption-Membrane Filtration Hybrid. *Desalination* **2011**, *283*, 193–197.
- (31) Kameda, T.; Oba, J.; Yoshioka, T. New Treatment Method for Boron in Aqueous Solutions Using Mg–Al Layered Double Hydroxide: Kinetics and Equilibrium Studies. *J. Hazard. Mater.* **2015**, *293*, 54–63.
- (32) Qiu, X.; Sasaki, K.; Takaki, Y.; Hirajima, T.; Ideta, K.; Miyawaki, J. Mechanism of Boron Uptake by Hydrocalumite Calcined at Different Temperatures. *J. Hazard. Mater.* **2015**, *287*, 268–277.
- (33) Chen, F.; Guo, L.; Zhang, X.; Leong, Z. Y.; Yang, S.; Yang, H. Y. Nitrogen-Doped Graphene Oxide for Effectively Removing Boron Ions from Seawater. *Nanoscale* **2017**, *9*, 326–333.
- (34) Tang, Y. P.; Chung, T. S.; Weber, M.; Maletzko, C. Development of Novel Diol-Functionalized Silica Particles toward Fast and Efficient Boron Removal. *Ind. Eng. Chem. Res.* **2017**, *56*, 11618–11627.
- (35) Palencia, M.; Vera, M.; Combatt, E. Polymer Networks Based in (4-Vinylbenzyl)-N-Methyl-D-Glucamine Supported on Microporous Polypropylene Layers with Retention Boron Capacity. *J. Appl. Polym. Sci.* **2014**, *131*, 40653.
- (36) Hansen, M. R.; Graf, R.; Spiess, H. W. Interplay of Structure and Dynamics in Functional Macromolecular and Supramolecular Systems As Revealed by Magnetic Resonance Spectroscopy. *Chem. Rev.* **2016**, *116*, 1272–1308.
- (37) Brown, S. P. Applications of High-Resolution ^1H Solid-State NMR. *Solid State Nucl. Magn. Reson.* **2012**, *41*, 1–27.
- (38) Cadars, S.; Allix, M.; Brouwer, D. H.; Shayib, R.; Suchomel, M.; Garaga, M. N.; Rakhmatullin, A.; Burton, A. W.; Zones, S. I.; Massiot, D.; Chmelka, B. F. Long- and Short-Range Constraints for the Structure Determination of Layered Silicates with Stacking Disorder. *Chem. Mater.* **2014**, *26*, 6994–7008.
- (39) Reddy, G. N. M.; Huqi, A.; Iuga, D.; Sakurai, S.; Marsh, A.; Davis, J. T.; Masiero, S.; Brown, S. P. Coexistence of Distinct Supramolecular Assemblies in Solution and in the Solid State. *Chem. - Eur. J.* **2017**, *23*, 2315–2322.
- (40) Peters, G. M.; Skala, L. P.; Plank, T. N.; Oh, H.; Reddy, G. N. M.; Marsh, A.; Brown, S. P.; Raghavan, S. R.; Davis, J. T. $\text{G}_4\text{-Quartet-M}^+$ Borate Hydrogels. *J. Am. Chem. Soc.* **2015**, *137*, 5819–5827.
- (41) Peters, G. M.; Skala, L. P.; Plank, T. N.; Hymann, B. J.; Reddy, G. N. M.; Marsh, A.; Brown, S. P.; Davis, J. T. A $\text{G}_4\text{-K}^+$ Hydrogel Stabilized by an Anion. *J. Am. Chem. Soc.* **2014**, *136*, 12596–12599.
- (42) Rossini, A. J.; Zagdoun, A.; Lelli, M.; Lesage, A.; Copéret, C.; Emsley, L. Dynamic Nuclear Polarization Surface Enhanced NMR Spectroscopy. *Acc. Chem. Res.* **2013**, *46*, 1942–1951.
- (43) Berruyer, P.; Lelli, M.; Conley, M. P.; Silverio, D. L.; Widdifield, C. M.; Siddiqi, G.; Gajan, D.; Lesage, A.; Copéret, C.; Emsley, L. Three-Dimensional Structure Determination of Surface Sites. *J. Am. Chem. Soc.* **2017**, *139*, 849–855.
- (44) Keeler, E. G.; Michaelis, V. K.; Colvin, M. T.; Hung, I.; Gor'kov, P. L.; Cross, T. A.; Gan, Z. H.; Griffin, R. G. O-17 MAS NMR Correlation Spectroscopy at High Magnetic Fields. *J. Am. Chem. Soc.* **2017**, *139*, 17953–17963.
- (45) Sangodkar, R. P.; Smith, B. J.; Gajan, D.; Rossini, A. J.; Roberts, L. R.; Funkhouser, G. P.; Lesage, A.; Emsley, L.; Chmelka, B. F. Influences of Dilute Organic Adsorbates on the Hydration of Low-Surface-Area Silicates. *J. Am. Chem. Soc.* **2015**, *137*, 8096–8112.
- (46) Lafon, O.; Thankamony, A. S. L.; Kobayashi, T.; Carnevale, D.; Vitzthum, V.; Slowing, I. I.; Kandel, K.; Vezin, H.; Amoureux, J. P.; Bodenhausen, G.; Pruski, M. Mesoporous Silica Nanoparticles Loaded with Surfactant: Low Temperature Magic Angle Spinning C-13 and Si-29 NMR Enhanced by Dynamic Nuclear Polarization. *J. Phys. Chem. C* **2013**, *117*, 1375–1382.
- (47) Kobayashi, T.; Perras, F. A.; Slowing, I. I.; Sadow, A. D.; Pruski, M. Dynamic Nuclear Polarization Solid-State NMR in Heterogeneous Catalysis Research. *ACS Catal.* **2015**, *5*, 7055–7062.
- (48) Lee, D.; Takahashi, H.; Thankamony, A. S. L.; Dacquain, J.-P.; Bardet, M.; Lafon, O.; De Paëpe, G. Enhanced Solid-State NMR Correlation Spectroscopy of Quadrupolar Nuclei Using Dynamic Nuclear Polarization. *J. Am. Chem. Soc.* **2012**, *134*, 18491–18494.
- (49) Leroy, C.; Aussenac, F.; Bonhomme-Courty, L.; Osaka, A.; Hayakawa, S.; Babonneau, F.; Coelho-Diogo, C.; Bonhomme, C. Hydroxyapatites: Key Structural Questions and Answers from Dynamic Nuclear Polarization. *Anal. Chem.* **2017**, *89*, 10201–10207.
- (50) Jantschke, A.; Koers, E.; Mance, D.; Weingarth, M.; Brunner, E.; Baldus, M. Insight into the Supramolecular Architecture of Intact Diatom Biosilica from DNP-Supported Solid-State NMR Spectroscopy. *Angew. Chem., Int. Ed.* **2015**, *54*, 15069–15073.
- (51) Corzilius, B.; Michaelis, V. K.; Penzel, S. A.; Ravera, E.; Smith, A. A.; Luchinat, C.; Griffin, R. G. Dynamic Nuclear Polarization of H-1, C-13, and Co-59 in a Tris(ethylenediamine)cobalt(III) Crystalline Lattice Doped with Cr(III). *J. Am. Chem. Soc.* **2014**, *136*, 11716–11727.
- (52) Karas, F.; Hnát, J.; Paidar, M.; Schauer, J.; Bouzek, K. Determination of the Ion-Exchange Capacity of Anion-Selective Membranes. *Int. J. Hydrogen Energy* **2014**, *39*, 5054–5062.
- (53) Lesage, A.; Lelli, M.; Gajan, D.; Caporini, M. A.; Vitzthum, V.; Miéville, P.; Alauzun, J.; Roussey, A.; Thieuleux, C.; Mehdi, A.; Bodenhausen, G.; Copéret, C.; Emsley, L. Surface Enhanced NMR Spectroscopy by Dynamic Nuclear Polarization. *J. Am. Chem. Soc.* **2010**, *132*, 15459–15461.
- (54) Lelli, M.; Gajan, D.; Lesage, A.; Caporini, M. A.; Vitzthum, V.; Miéville, P.; Héroguel, F.; Rascón, F.; Roussey, A.; Thieuleux, C.; Boualleg, M.; Veyre, L.; Bodenhausen, G.; Copéret, C.; Emsley, L. Fast Characterization of Functionalized Silica Materials by Silicon-29 Surface-Enhanced NMR Spectroscopy Using Dynamic Nuclear Polarization. *J. Am. Chem. Soc.* **2011**, *133*, 2104–2107.
- (55) Zagdoun, A.; Casano, G.; Ouari, O.; Schwarzwälder, M.; Rossini, A. J.; Aussenac, F.; Yulikov, M.; Jeschke, G.; Copéret, C.; Lesage, A.; Tordo, P.; Emsley, L. Large Molecular Weight Nitroxide Biradicals Providing Efficient Dynamic Nuclear Polarization at Temperatures up to 200 K. *J. Am. Chem. Soc.* **2013**, *135*, 12790–12797.
- (56) Rankin, A. G. M.; Trébosc, J.; Pourpoint, F.; Amoureux, J.-P.; Lafon, O. Recent Developments in MAS DNP-NMR of Materials. *Solid State Nucl. Magn. Reson.* **2019**, *101*, 116–143.
- (57) Zagdoun, A.; Rossini, A. J.; Gajan, D.; Bourdolle, A.; Ouari, O.; Rosay, M.; Maas, W. E.; Tordo, P.; Lelli, M.; Emsley, L.; Lesage, A.; Copéret, C. Non-Aqueous Solvents for DNP Surface Enhanced NMR Spectroscopy. *Chem. Commun.* **2012**, *48*, 654–656.
- (58) Rosay, M.; Tometich, L.; Pawsey, S.; Bader, R.; Schauwecker, R.; Blank, M.; Borchard, P. M.; Cauffman, S. R.; Felch, K. L.; Weber, R. T.; Temkin, R. J.; Griffin, R. G.; Maas, W. E. Solid-State Dynamic Nuclear Polarization at 263 GHz: Spectrometer Design and Experimental Results. *Phys. Chem. Chem. Phys.* **2010**, *12*, 5850–5860.
- (59) Schnell, I.; Lupulescu, A.; Hafner, S.; Demco, D. E.; Spiess, H. W. Resolution Enhancement in Multiple-Quantum MAS NMR Spectroscopy. *J. Magn. Reson.* **1998**, *133*, 61–69.
- (60) Hayashi, S.; Hayamizu, K. Chemical Shift Standards in High-Resolution Solid-State NMR (2) ^{15}N Nuclei. *Bull. Chem. Soc. Jpn.* **1991**, *64*, 688–690.
- (61) Harris, R. K.; Becker, E. D.; Cabral De Menezes, S. M.; Granger, P.; Hoffman, R. E.; Zilm, K. W. Further Conventions for NMR Shielding and Chemical Shifts (IUPAC Recommendations 2008). *Pure Appl. Chem.* **2008**, *80*, 59–84.
- (62) Martin, G. E.; Hadden, C. E. Long-Range ^1H - ^{15}N Heteronuclear Shift Correlation at Natural Abundance. *J. Nat. Prod.* **2000**, *63*, 543–585.

- (63) Bertani, P.; Raya, J.; Bechinger, B. N-15 Chemical Shift Referencing in Solid State NMR. *Solid State Nucl. Magn. Reson.* **2014**, *61–62*, 15–18.
- (64) Martin, G. J.; Martín, M. L.; Gouesnard, J. P. *¹⁵N-NMR Spectroscopy*; Springer: 1981.
- (65) Wong, T. C.; Collazo, L. R.; Guziec, F. S. ¹⁴N and ¹⁵N NMR Studies of Highly Sterically Hindered Tertiary Amines. *Tetrahedron* **1995**, *51*, 649–656.
- (66) Hušák, M.; Jegorov, A.; Rohlíček, J.; Fitch, A.; Czernek, J.; Kobera, L.; Brus, J. Determining the Crystal Structures of Peptide Analogs of Boronic Acid in the Absence of Single Crystals: Intricate Motifs of Ixazomib Citrate Revealed by XRPD Guided by ss-NMR. *Cryst. Growth Des.* **2018**, *18*, 3616–3625.
- (67) Brus, J.; Czernek, J.; Urbanova, M.; Kobera, L.; Jegorov, A. An Efficient 2D B-11-B-11 Solid-State NMR Spectroscopy Strategy for Monitoring Covalent Self-Assembly of Boronic Acid-Derived Compounds: The Transformation and Unique Architecture of Bortezomib Molecules in the Solid State. *Phys. Chem. Chem. Phys.* **2017**, *19*, 487–495.
- (68) Weiss, J. W. E.; Bryce, D. L. A Solid-State B-11 NMR and Computational Study of Boron Electric Field Gradient and Chemical Shift Tensors in Boronic Acids and Boronic Esters. *J. Phys. Chem. A* **2010**, *114*, 5119–5131.
- (69) Hough, A.; Routh, A. F.; Clarke, S. M.; Wiper, P. V.; Amelse, J. A.; Mafra, L. Boron Removal and Reinsertion Studies in ¹⁰B–¹¹B Exchanged HAMS-1B (H-[B]-ZSM-5) Borosilicate Molecular Sieves Using Solid-State NMR. *J. Catal.* **2016**, *334*, 14–22.
- (70) Harada, A.; Takagi, T.; Kataoka, S.; Yamamoto, T.; Endo, A. Boron Adsorption Mechanism on Polyvinyl Alcohol. *Adsorption* **2011**, *17*, 171–178.
- (71) Joshi, M. D.; Chalumot, G.; Kim, Y.-w.; Anderson, J. L. Synthesis of Glucaminium-Based Ionic Liquids and Their Application in the Removal of Boron from Water. *Chem. Commun.* **2012**, *48*, 1410–1412.

Nanoscale surface compositions and structures influence boron adsorption properties of anion exchange resins

G. N. Manjunatha Reddy,¹ Jeffrey A. Gerbec,² Fumihiko Shimizu,³ Bradley F. Chmelka^{1,*}

¹ *Department of Chemical Engineering, University of California, Santa Barbara, California, 93106, U.S.A.*

² *Mitsubishi Chemical–Center for Advanced Materials, University of California, Santa Barbara, California, 93106, U.S.A.*

³ *Science and Innovation Center, Mitsubishi Chemical Corporation, Yokohama-shi, Kanagawa 227-8502, Japan*

Electronic Supplementary Information

Table of contents

1. Inductively-Coupled-Plasma atomic emission spectroscopy of a NMDG-functionalized resin
2. 1D ¹⁵N{¹H} DNP-NMR spectra of NMDG and boron-adsorbed NMDG-functionalized resin
3. 1D ¹¹B{¹H} CP–MAS NMR spectra of boron-adsorbed NMDG-functionalized resin
4. Solid-state 1D ¹H, 2D ¹³C{¹H} HETCOR and 2D ¹H{¹H} DQ-SQ correlation NMR spectra of NMDG, PSDVB resin, and NMDG-functionalized resin
5. XPS analyses of different batches of boron-adsorbed NMDG-functionalized resins
6. 1D ¹⁵N{¹H} DNP-NMR spectra of different batches of boron-adsorbed NMDG-functionalized resins
7. Boron adsorption behaviors of different batches of NMDG-functionalized resins
8. Solid-state 2D ¹¹B{¹H} and ¹³C{¹H} correlation NMR spectra of different NMDG-functionalized resins.

1. Inductively-Coupled-Plasma atomic emission spectroscopy of NMDG-functionalized PSDVB resins

Table S1. Elemental concentrations of metal ions in NMDG-functionalized resins

Concentration (Equivalents)	NMDG-functionalized resin	
	Before boron exposure	After boron exposure
B	<1	2500
Na	<10	<10
Mg	<1	<1
Al	<1	<1
Ca	<10	<10
Fe	<10	<10
Ni	<1	<1
Zn	<1	<1

Upon treatment with Millipore water, the ^{11}B signal originate from the mono-chelate complex was observed to be less intense relative to the ^{11}B signal from the bis-chelate complex. This is attributed to relatively weak affinity interactions of borate anions in *mono*-chelate complexes in comparison to the borate anions in *bis*-chelate complexes. The borate anions in *mono*-chelate are thus more likely to exchange with counter ions in aqueous solutions as previously observed by Davis and co-workers, for example, in guanosine borate gels [Refs. 40 and 41 of the main paper].

2. 1D $^{15}\text{N}\{^1\text{H}\}$ DNP-MAS NMR spectra of boron-adsorbed NMDG-functionalized resins and precursor species.

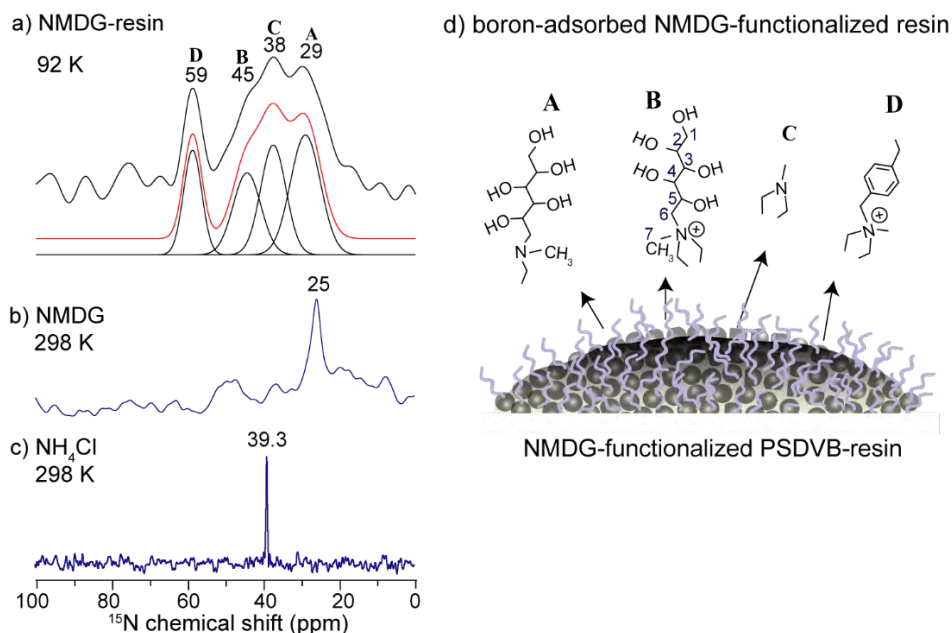


Figure S1. Surface-enhanced 1D $^{15}\text{N}\{^1\text{H}\}$ DNP-MAS NMR spectra acquired at 9.4 T, 92 K, and 8 kHz MAS, with a CP contact time of 2 ms and using 16 mM TEKPol in 1,1,2,2-tetrachloroethane on (a) NMDG-functionalized ion-exchange resin acquired using 16384 co-added transients and a relaxation delay of 4 s corresponding to a total experimental time of 18 h and (b) NMDG acquired using 8192 co-added transients and a relaxation delay of 4 s corresponding to a total experimental time of 9 h. (c) Conventional 1D $^{15}\text{N}\{^1\text{H}\}$ CP-MAS NMR spectra of powdered NH_4Cl acquired under similar conditions, though at 298 K, using 512 co-added transients and a CP contact time of 1 ms and relaxation delay of 4 s corresponding to a total experimental time of 35 m. ^{15}N signal assignments of surface species **A**, **B**, **C**, or **D** are labelled as indicated in (d) the schematic diagram of the functional groups on the resin surface.

3. 1D $^{11}\text{B}\{^1\text{H}\}$ CP-MAS NMR spectra of NMDG-functionalized resins

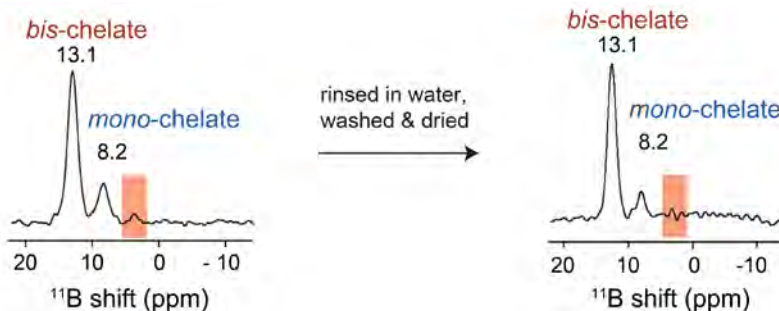


Figure S2. Solid-state 1D $^{11}\text{B}\{^1\text{H}\}$ CP-MAS NMR spectra acquired at 11.7 T and at room temperature of NMDG-functionalized resins containing adsorbed boron (a) before and (b) after washing with ultrapure water. Assignments of borate *mono*- (8.2 ppm) and *bis*-chelate (13.1 ppm) complexes and non-covalently bound boron atoms (3.2 ppm) are labeled above the respective signals or by the shaded bands.

4. Solid-state 1D ^1H , 2D $^{13}\text{C}\{^1\text{H}\}$ HETCOR and 2D $^1\text{H}\{^1\text{H}\}$ DQ-SQ correlation NMR spectra of NMDG, PSDVB resin, and NMDG-functionalized resin

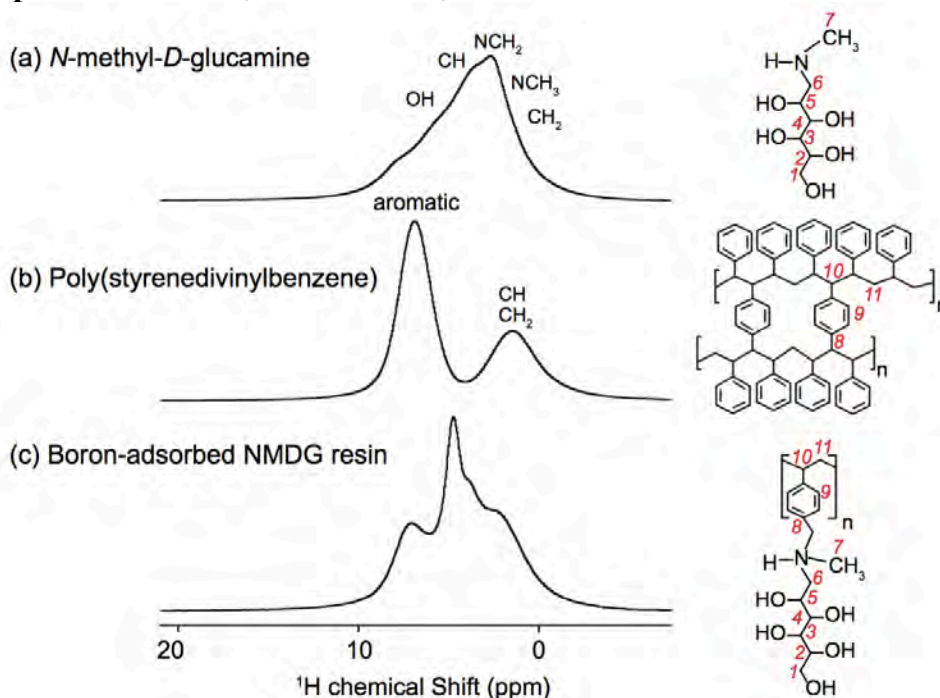


Figure S3. Solid-state 1D ^1H MAS NMR spectra acquired at 11.7 T, 298 K, and 60 kHz MAS of (a) NMDG, (b) PSDVB resin, and (c) boron-adsorbed NMDG-functionalized PSDVB resin. Assignments of ^1H signals associated with alkyl and aromatic groups are indicated that are accompanied by the schematic structure figures (right).

Dipole-dipole-coupled ^{13}C - ^1H moieties can be distinguished and identified by recording 2D $^{13}\text{C}\{^1\text{H}\}$ heteronuclear correlation (HETCOR) NMR spectra at different CP contact times. Improved resolution is achieved in the indirect ^1H dimension of the 2D $^{13}\text{C}\{^1\text{H}\}$ HETCOR spectra of NMDG (Figure S4), which enabled different ^1H signals to be distinguished and assigned. In particular, strong intensity correlations associated with dipole-dipole-coupled ^{13}C - ^1H moieties in the 2D $^{13}\text{C}\{^1\text{H}\}$ HETCOR spectrum of NMDG (Figure S4a) acquired using a short 0.1 ms contact time establishes spatial proximities of ^{13}C - ^1H pairs in terminal $-\text{NCH}_3$ ($C7$ 38 ppm and $H7$ 1.2 ppm), $-\text{NCH}_2$ ($C6$ 56 ppm and ^1H 1.5 ppm), central $-\text{CH}-$ ($C2$ 74, $C3$ 68, $C4$ - 5 71 ppm and $H2$ - 5 2.6 ppm) groups and $-\text{CH}_2\text{OH}$ ($C1$ 62 ppm and ^1H 1.5 ppm) moieties. In addition, 2D correlation intensities between ^{13}C signals ($C2$ - $C6$) and ^1H signal at 4.2 ppm indicate close proximities between carbon atoms and hydroxyl groups. A 2D $^{13}\text{C}\{^1\text{H}\}$ HETCOR spectrum of NMDG was acquired under identical conditions, except using a longer 2 ms contact time (Figure S4b); it establishes spatial proximities of ^{13}C - ^1H pairs between central carbon atoms and $-\text{NH}$ (6.5 ppm) groups and central carbon atoms and OH groups (8.1 ppm) moieties. The high ppm value of OH (8.1 ppm) is attributed to strong hydrogen-bonding interactions between hydroxyl groups of neighboring NMDG moieties. Notably, ^1H chemical shifts of $-\text{OH}$ (4.5 ppm), $-\text{NH}$ (6.1 ppm) and hydrogen-bonded $-\text{OH}$ groups (8.1 ppm) are clearly resolved in the ^1H dimension of the 2D $^{13}\text{C}\{^1\text{H}\}$ HETCOR spectrum.

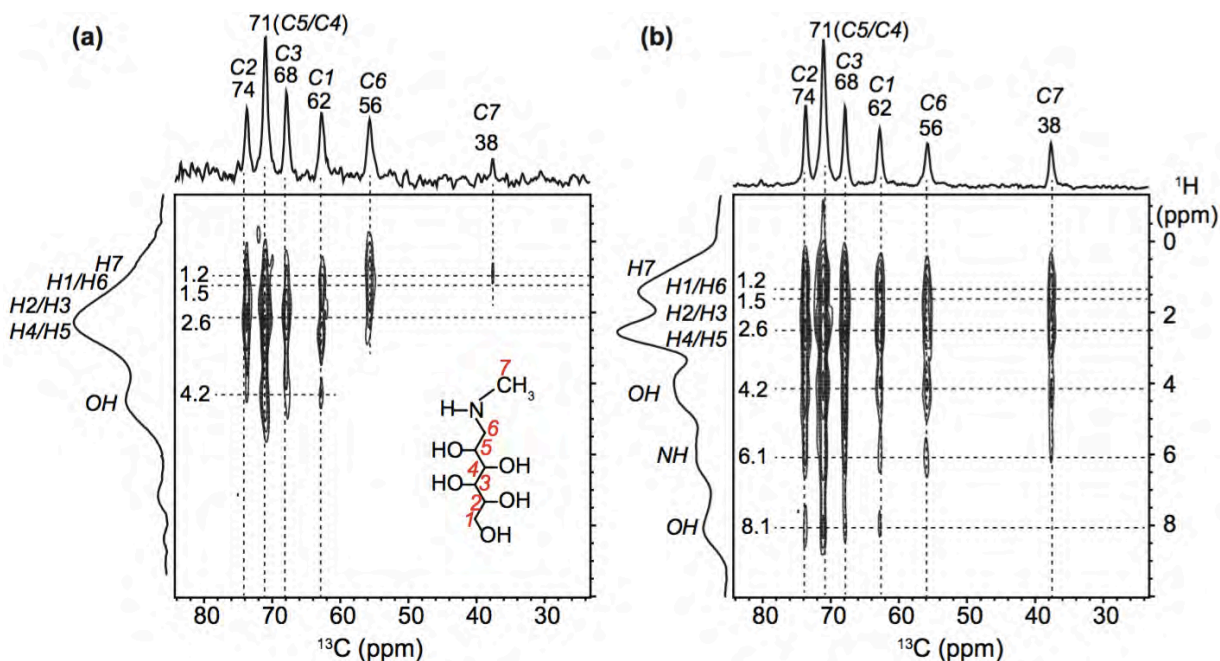


Figure S4. 2D $^{13}\text{C}\{^1\text{H}\}$ HETCOR NMR spectra of *N*-methyl-*D*-glucamine, which were recorded at 11.7 T, room temperature, 12.5 kHz MAS, and with a CP contact time of (a) 0.1 ms or (b) 2 ms. Projections of the 2D ^{13}C and ^1H intensities are shown along the top horizontal and left vertical axes, respectively. Dashed lines depict the ^{13}C - ^1H signal assignments, with numbering as shown in the accompanying schematic diagram.

Concurrently, correlated 2D intensities observed in the 2D $^{13}\text{C}\{^1\text{H}\}$ HETCOR NMR spectrum of PSDVB resin (Figure S5a) acquired using a short contact time of 0.1 ms are characteristic of dipole-dipole couplings between directly bonded ^{13}C - ^1H pairs; correlated signals of *C10* (41 ppm), *C11* (47 ppm) and ^1H signals of 1.5 ppm correspond to vinyl – CH and – CH₂ groups, and between ^{13}C signals of *C9* at 129 ppm and ^1H signals at 6.7 ppm originate from benzyl groups. In the 2D $^{13}\text{C}\{^1\text{H}\}$ HETCOR NMR spectrum (Figure S5b) of PSDVB resin acquired using a longer contact time of 2 ms, correlated 2D intensities between *C10* (41 ppm), *C11* (47 ppm) and aromatic ^1H signals of 6.7 ppm and between *C9* carbon atoms (129 ppm) and ^1H signals vinyl – CH and – CH₂ groups, and between ^{13}C signals at 129 ppm and ^1H signals at 6.7 ppm originate from benzyl groups at 1.5 ppm are observed, which indicate long-range dipole-dipole interactions between aromatic and vinyl groups of PSDVB resin. These 2D correlated intensities establish that the aromatic carbon atoms are spatially proximate (< 1 nm) to the benzylic and methylene hydrogen atoms. Analyses of 2D $^{13}\text{C}\{^1\text{H}\}$ HETCOR NMR spectra of NMDG and PSDVB provide an indispensable basis to separate to distinguish and identify 2D correlation intensities in the analogues HETCOR spectra of boron-adsorbed NMDG-resin acquired using short (0.1 ms) and long (2 ms) of contact times, as shown in Figure S6, which will be discussed in the next section.

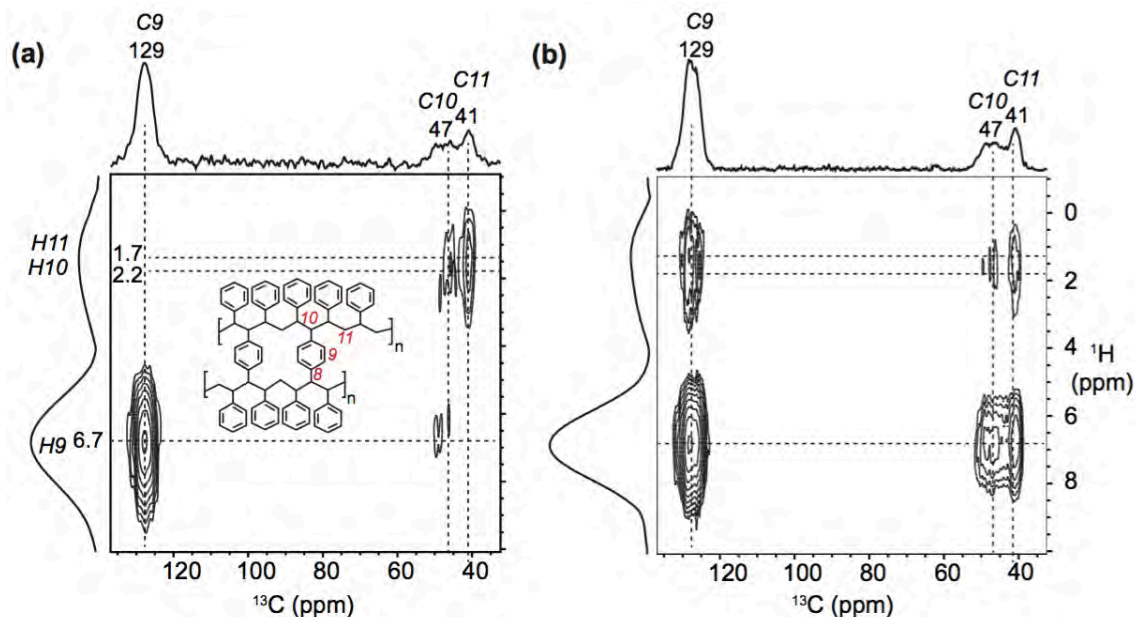


Figure S5. 2D $^{13}\text{C}\{^1\text{H}\}$ HETCOR NMR spectra of PSDVB, which were acquired at 11.7 T, 298 K, 12.5 kHz MAS, and with a CP contact time of (a) 0.1 ms or (b) 2 ms. Projections of ^{13}C and ^1H spectra are shown along the top horizontal and left vertical axes, respectively. Dashed lines depict the ^{13}C - ^1H signal assignments.

To gain insight into the local structures of chelate complexes and mutual interactions between boron atoms and the functional groups on the resin particle surface, 2D $^{13}\text{C}\{^1\text{H}\}$ HETCOR NMR and $^1\text{H}\{^1\text{H}\}$ DQ-SQ correlation spectra of a boron-adsorbed NMDG-functionalized PSDVB resin was analyzed and compared (Figures S6 and S7). In the 2D $^{13}\text{C}\{^1\text{H}\}$ HETCOR spectrum recorded using a short recoupling time of 0.1 ms, broad distributions of ^{13}C NMR signals at 40-45 ppm (*C10*, *C11*) and ^{13}C NMR signals at 1.2–2.2 ppm (*H10*, *H11*) originate from the vinyl groups, and distributions of correlations between ^{13}C signals in the range 125-135 ppm (*C9*) and ^1H signals at 6.7 ppm correspond to aromatic groups of the PSDVB resin, respectively. Whereas, a broad distribution of 2D correlations between ^{13}C signal intensities in the range 60-75 ppm (*C1-C6*) and ^1H signals in the range 2.2-4.1 (*H1-H6*) ppm is attributed to the directly bonded ^{13}C - ^1H pairs in the of the surface-grafted NMDG groups on the PSDVB resin. By comparison, 2D $^{13}\text{C}\{^1\text{H}\}$ HETCOR spectrum recorded using a short recoupling time of 2 ms exhibited correlated 2D intensities stemming from long-range ^{13}C - ^1H dipole-dipole interactions between NMDG surface functional groups and the PSDVB resin. For example, distributions of 2D correlation intensities between ^{13}C signals in the range of 60-75 ppm and ^1H signals at 6.7 ppm, and between ^{13}C signals at 125-135 ppm and ^1H signals at 2.2-4.1 ppm indicate the close proximities (< 1 nm) between NMDG surface functional groups and PSDVB resin. In particular, subtle differences and broad distributions of correlated 2D intensities of ^{13}C - ^1H moieties in surface-grafted NMDG moieties (Figure S6a) in comparison to the analogue 2D correlations of NMDG moieties (Figure S4a) is attributed to the surface heterogeneity associated with grafted NMDG moieties on the PSDVB resin. In addition, the absence of ^{13}C - ^1H correlated 2D intensities between NMDG carbon atoms (*C1-C5*, 60-57 ppm) and hydrogen bonded protons of hydroxyl groups (*OH*, 8.1 ppm) is due to the lack of hydroxyl groups upon the formation of boron chelate complexes.

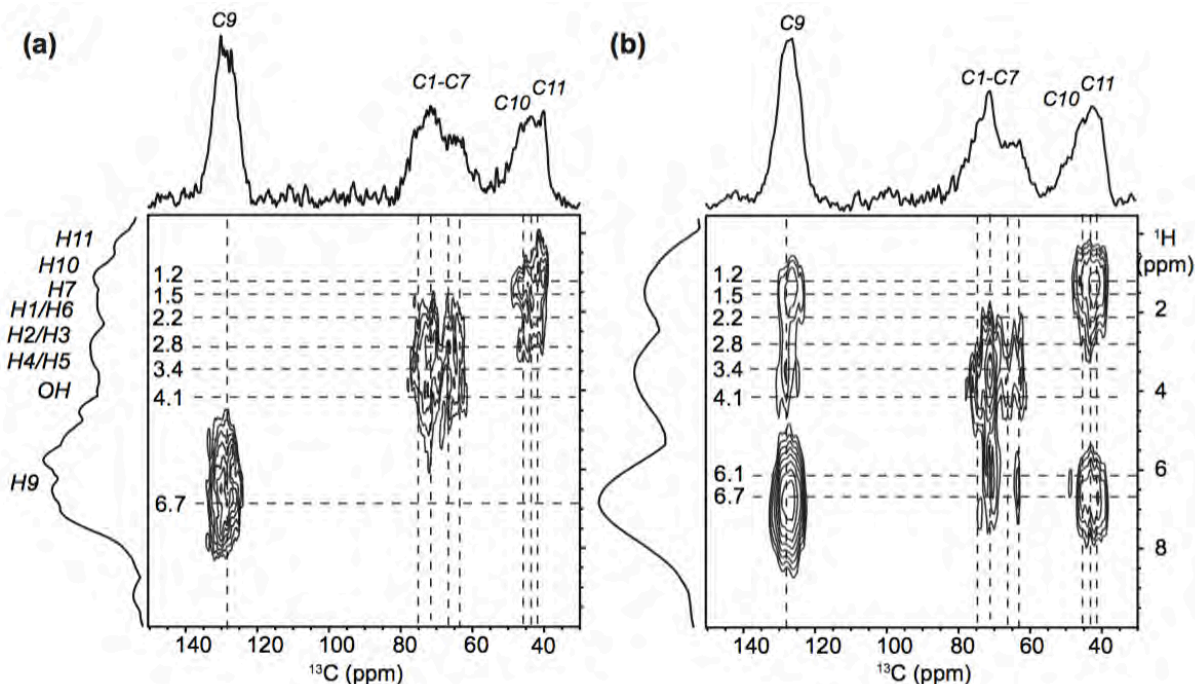


Figure S6. 2D $^{13}\text{C}\{^1\text{H}\}$ HETCOR NMR spectra of boron-adsorbed PSDVB-NMDG-resin, which were recorded at 11.7 T, room temperature, 12.5 kHz MAS, and with a CP contact time of (a) 0.1 ms or (b) 2 ms. Projections of ^{13}C and ^1H spectra are shown along the top horizontal and left vertical axes, respectively. Dashed lines depict assignments of 2D ^{13}C - ^1H correlation intensities.

Molecularly proximate and dipole-dipole-coupled ^1H - ^1H pairs can be probed by analyzing 2D $^1\text{H}\{^1\text{H}\}$ double-quantum – single-quantum (DQ-SQ) correlation NMR spectra of NMDG functional groups, PSDVB resin, and boron-adsorbed NMDG-functionalized PSDVB resins (Figure S7). In the 2D ^1H DQ-SQ NMR spectrum of NMDG (Figure S7a, gray color dots), self-correlation intensities correspond to CH_2 (SQ = 1.2 and DQ = 2.4 ppm), NCH_3 (SQ = 1.5 and DQ = 3.0 ppm), NCH_2 (SQ = 2.6 and DQ = 5.2 ppm) and NH (SQ = 4.2 and DQ = 8.2 ppm) and NH (SQ = 6.1 and DQ = 12.2 ppm) moieties, and cross-correlated 2D intensities associated with NCH_3 and NH (DQ = 6.0 ppm), NCH_2 and NH (DQ = 7.1 ppm) are observed (Table S2). By comparison, in the 2D ^1H DQ-SQ NMR spectrum of PSDVB resin (Figure S7b, green color dots), self-correlation intensities at SQ = 1.7 and DQ = 3.4 ppm, SQ = 2.2 and DQ = 4.4 ppm and at SQ = 6.7 and DQ = 13.4 ppm correspond to ^1H - ^1H proximities in vinyl and aromatic groups. In addition, and cross-correlated 2D intensities at 8.4 and 8.9 ppm in the DQ dimension associated with ^1H - ^1H proximities between vinyl and aromatic groups of PSDVB are observed. Analyses of 2D $^1\text{H}\{^1\text{H}\}$ spectra of NMDG and PSDVB spectra enable distinct 2D correlation intensities in the 2D $^1\text{H}\{^1\text{H}\}$ DQ-SQ spectra of boron-adsorbed NMDG-resin to be distinguished and identified. Likewise, in the NMDG-functionalized PSDVB resin, the assignments of 2D self-correlation intensities associated with NMDG and PSDVB moieties are realized and depicted in colored gray (NMDG) and green (PSDVB) dots, which is consistent with the analyses of the 2D $^{13}\text{C}\{^1\text{H}\}$ and $^{11}\text{B}\{^1\text{H}\}$ HETCOR NMR spectra of boron-adsorbed resins discussed in the previous sections.

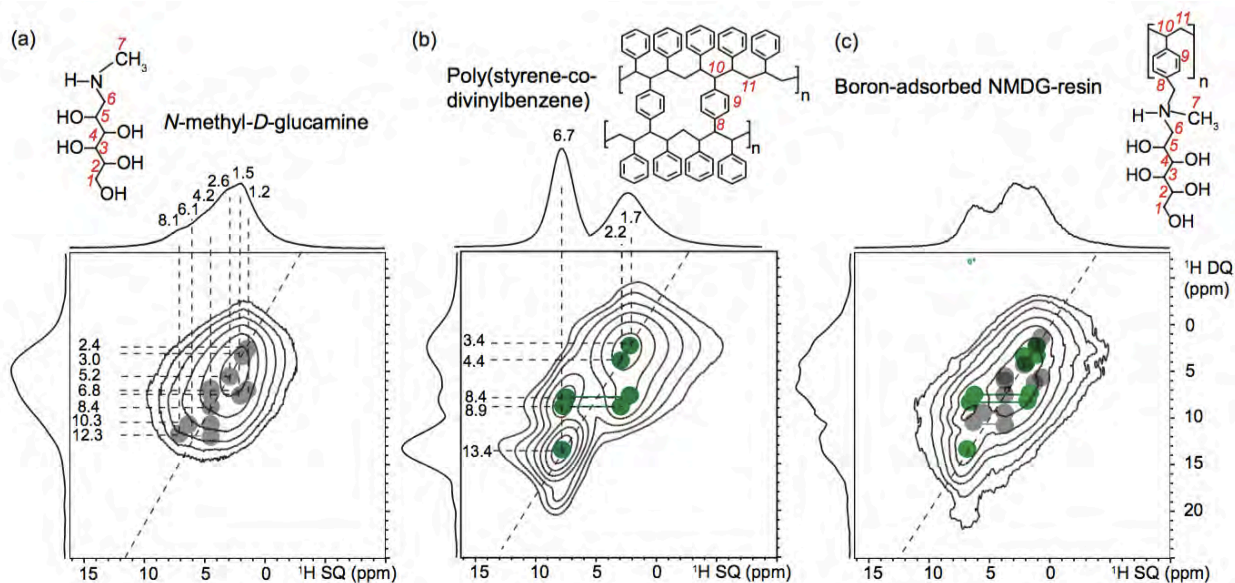


Figure S7. Solid-state 2D $^1\text{H}\{^1\text{H}\}$ DQ-SQ NMR correlation spectra acquired at 11.7 T, 298 K and 60 kHz MAS of (a) NMDG, (b) PSDVB resin, and (c) boron-adsorbed NMDG-functionalized PSDVB resin. The corresponding 1D ^1H double-quantum filtered (DQF) MAS spectra are shown along the top horizontal axes. Correlated signal intensity originates from dipolar-coupled ^1H - ^1H pairs are depicted by gray (NMDG) and green color (PSDVB) circles.

Table S2. Experimental ^1H SQ and DQ chemical shifts of NMDG and PSDVB resin

Chemical site	^1H SQ (ppm)	^1H DQ (ppm)
<i>N</i> -methyl- <i>D</i> -glucamine (NMDG)		
CH ₂ +CH ₂	1.2+1.2	2.4
NCH ₃ + NCH ₃	1.5+1.5	3.0
NCH ₂ +NCH ₂	2.6+2.6	5.2
NH+NCH ₃	4.2+1.5	6.0
NH+NCH ₂	4.2+2.6	7.1
NH+NH	4.2+4.2	9.0
OH+OH	6.1+4.2	10.6
OH+OH	8.1+4.2	12.6
Poly(styrene-co-divinylbenzene) (PSDVB)		
CH ₂ +CH ₂	1.5+1.5	3.0
CH ₂ +CH	1.5+2.2	3.7
CH+CH	2.2+2.2	4.4
CH _{aromatic} +CH ₂	6.8+1.7	8.5
CH _{aromatic} +CH	6.8+2.2	9.0
CH _{aromatic} +CH _{aromatic}	6.8+6.8	13.6

5. XPS analyses of NMDG-functionalized ion exchange resins with adsorbed boron for different batches

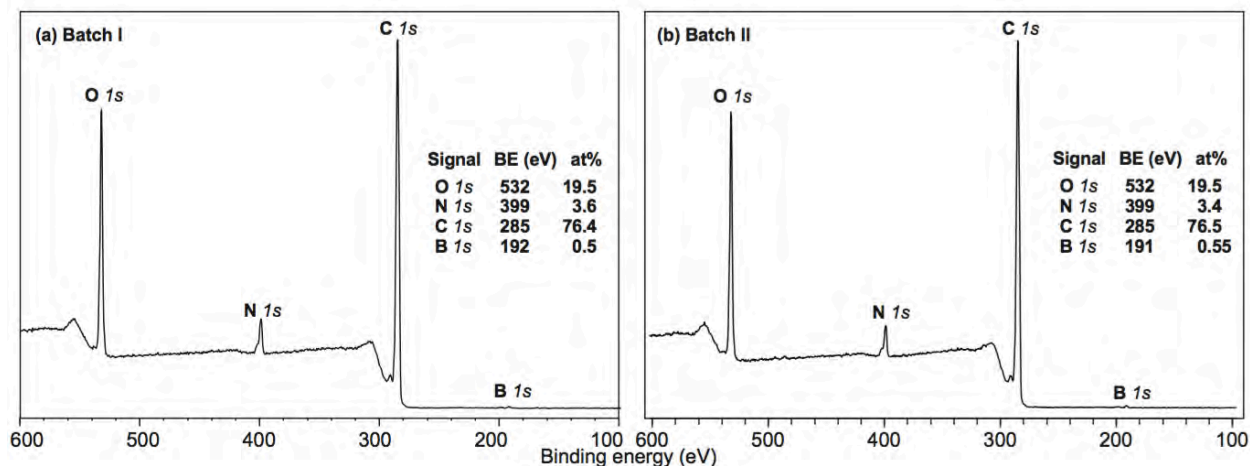


Figure S8. Survey scan XPS spectra acquired at room temperature for (a) Batch I and (b) Batch II boron-adsorbed NMDG-resins with signal intensities at 532, 399, 285 and 191 eV assigned to O 1s, N 1s, C 1s and B 1s. The elemental compositions of O, N, C and B atoms are shown in the inset Tables and fitting parameters are given in Table S3, which depict subtle differences in the composition of N.

Table S3. Binding energy values determined by XPS and elemental concentrations of O, N, C and B atoms for Batch I and Batch II boron-adsorbed NMDG-functionalized resins.

Element	Binding energy (eV)	Full width at half maximum	Area	At%
Batch I				
O 1s	532.0	2.52	10668.29	19.50
N 1s	399.0	2.34	1516.79	3.39
C 1s	285.0	3.01	19018.95	76.48
B 1s	191.0	2.13	70.18	0.5
Batch II				
O 1s	532.0	2.55	11723.02	19.51
N 1s	399.0	2.43	1789.03	3.64
C 1s	284.5	2.97	20866.41	76.39
B 1s	192.0	2.13	83.33	0.55

6. 1D $^{15}\text{N}\{^1\text{H}\}$ DNP-NMR analyses of different batches of NMDG-functionalized resins

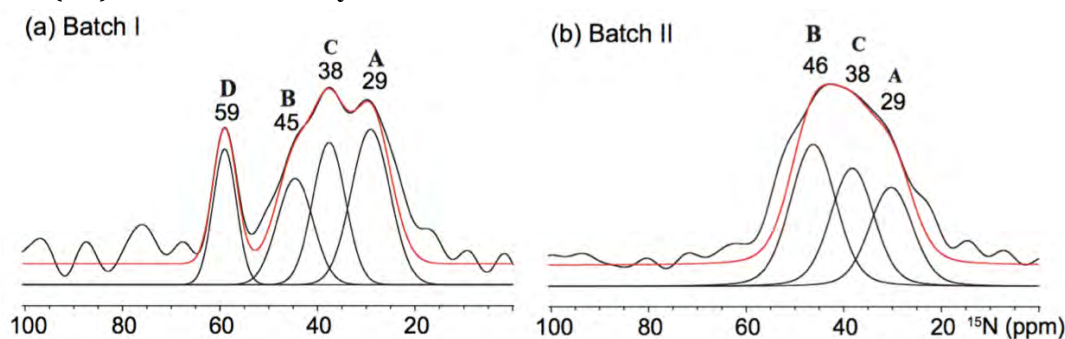


Figure S9. Surface-enhanced 1D $^{15}\text{N}\{^1\text{H}\}$ DNP-MAS NMR spectra for (a) Batch I and (b) Batch II resins after boron exposure, which manifest different distributions of surface nitrogen species. The spectra were acquired at 9.4 T (^1H 400 MHz, ^{15}N 40.6 MHz), 92 K, 8 kHz MAS with a CP contact time of 2 ms and using 16 mM TEKPol in 1,1,2,2-tetrachloroethane.

Table S4. Deconvoluted signal integrals and lineshape analyses of surface-enhanced 1D $^{15}\text{N}\{^1\text{H}\}$ DNP MAS NMR spectra of NMDG-functionalized Batch I and II resins.

Deconvolution parameters		Batch I				Batch II		
Chemical shift (ppm)	59	45	38	29	46	38	29	
Gaussian broadening (Hz)	230	360	340	380	460	460	460	
Normalized signal integrals (a.u.)	1.0	1.2	1.4	1.9	1.0	0.7	0.5	
Densities of exchange sites ($\pm 5\%$)	18	22	26	34	46	32	22	

7. Boron adsorption behaviors of different batches of NMDG-functionalized resins

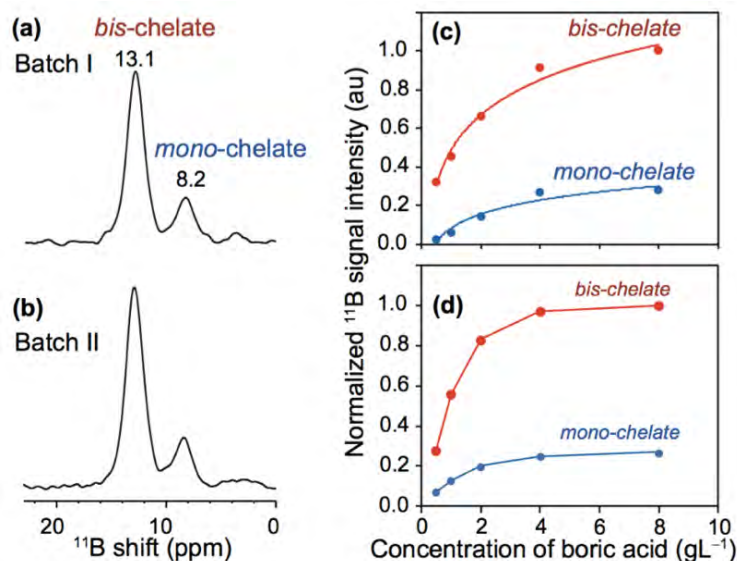


Figure S10. Solid-state $^{11}\text{B}\{^1\text{H}\}$ CP-MAS NMR spectra acquired at 11.7 T, 298 K, and 8 kHz MAS using CP contact time of 2 ms for (a) Batch I and (b) Batch II boron-adsorbed NMDG-functionalized resins. ^{11}B signal assignments are shown for *mono*- and *bis*-chelate complexes. (c,d) Plots of normalized $^{11}\text{B}\{^1\text{H}\}$ CP signal intensity, as functions of boric acid concentration for (c) Batch I and (d) Batch II resins.

8. Solid-state 2D $^{11}\text{B}\{^1\text{H}\}$ and $^{13}\text{C}\{^1\text{H}\}$ correlation NMR spectra of different NMDG-functionalized resins.

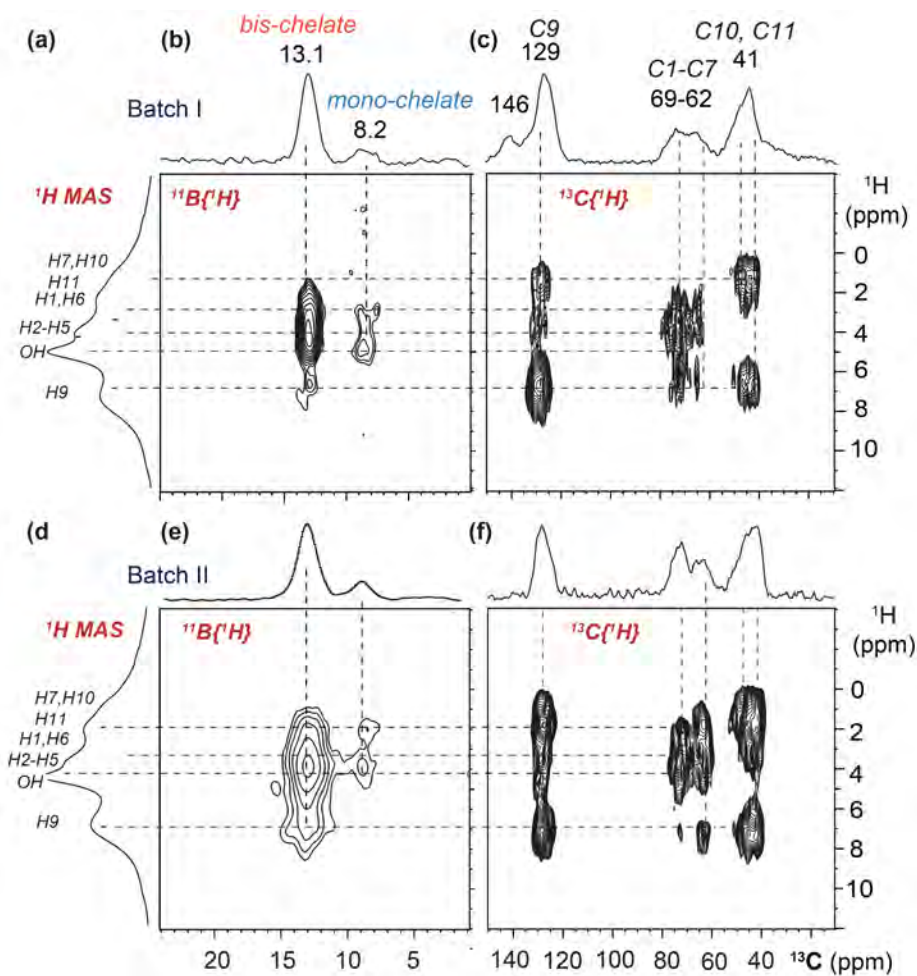


Figure S11. Solid-state 1D ^1H MAS NMR spectra acquired at 11.7 T, room temperature, and 60 kHz MAS and 2D $^{11}\text{B}\{^1\text{H}\}$ and $^{13}\text{C}\{^1\text{H}\}$ heteronuclear correlation NMR spectra acquired under identical conditions expect using 12.5 kHz MAS of (top; a, b, c) Batch I and (bottom; d, e, f) Batch II boron-adsorbed NMDG-resins. 2D $^{11}\text{B}\{^1\text{H}\}$ and $^{13}\text{C}\{^1\text{H}\}$ correlation intensities indicate the presence of *mono*- and *bis*-chelate complexes on the resin surfaces, which establish that the boron adsorption occurs through the formation of chelate complexes.